


Facultatea de Inginerie Chimică și Biotehnologii

UNIVERSITY „POLITEHNICA" of BUCHAREST

FACULTY of CHEMICAL ENGINEERING and BIOTECHNOLOGIES

Doctorate

Application of ultrasound and microwaves in the catalyst's synthesis, catalytic processes development and extraction of active principles

Aplicarea ultrasunetelor și microundelor în sinteza catalizatorilor, desfășurarea proceselor catalitice și extracția de principii active

SUMMARY of the doctoral thesis

REZUMAT al Tezei

PhD supervisor:
Prof. Dr. Eng. Ioan Călinescu

Author:
Eng. Ciprian-Gabriel Chisega-Negrilă

Bucharest, 2022

Thesis' SUMMARY

	ABREVIATIONS	.....	6
A.	**Literature studies**	.....	11
I.	**Biomass-derived building blocks and key intermediates**	.....	12
II.	**n-Butanol – a new biomass-derived building block**	.....	32
III.	**Dry/wet reforming of methane with carbon dioxide**	.....	46
IV.	**Microwave**	.....	105
V.	**Liquorice root – *Glycyrrhiza glabra* – Valorization by extraction of active compounds**	.....	129
B.	**Experimental Phase**	.....	136
VI.	**Conversion of n-bio-Butanol to Butyraldehyde – Screening of copper catalysts – Effect of catalyst synthesis method on the dehydrogenation of n-bio-Butanol**	.....	137
VII.	**Catalytic activity of some nickel catalysts tested for synthesis gas production in the dry and wet reforming reaction of hydrocarbons: methane and liquefied petroleum gas with carbon dioxide**	.....	166
VIII.	**Experiments on cascade extraction of Liquorice waste – *Glycyrrhiza glabra* – for process intensification by severe ultrasound and microwave treatments**	.....	217
	ANNEX I	.....	225
	Conclusions	.....	241
	Perspectives	.....	242
	Original Contributions	.....	243
	Dissemination of results	.....	247
	Bibliography	.....	248

SUMMARY

Chapter I.

Conversion of n-bio-Butanol to Butyraldehyde – Screening of copper catalysts – Effect of the catalyst synthesis method on the dehydrogenation of n-bio-Butanol

OBJECTIVES

O1. Highlighting the support's acidity effect on the catalytic activity of the catalyst for a wide range of copper catalysts;

O2. Establishing the effect of the ultrasound application within the synthesis method of the catalyst through wet impregnation

I.1. Introduction

In the current context in which organic chemistry gathers its forces for a new offensive, catalysis is undergoing a period of revitalization in its attempt to produce new catalysts with improved performance.
The supported catalysts obtained through conventional wet impregnation methods [1, 2] begin to be replaced with supported catalysts prepared by innovative, nonconventional techniques [3, 4] involving ultrasounds [5-8] and/or microwaves [9]. The latter have the potential to provide conversions and selectivities to useful products which are superior to the supported catalysts achieved by conventional methods. The catalysts prepared by conventional wet impregnation method differs from the catalysts prepared by innovative, nonconventional technique because in this case ultrasounds are applied in the contacting phase. Ultrasonic technique is used on a large scale for a wide range of chemical reactions and processes [10], and it is now recognized as a branch of chemistry, namely-sonochemistry [11-14]. The core of sonochemical reactions is the cavitational bubbles generated during sonication of a liquid. In principle, there are two types of cavitational collapsing bubbles: symmetrical and asymmetrical ones. The collapse of a symmetrical bubble (see **Fig. 1.1.a**) generates local high temperature and pressure [15], while the asymmetrical bubble collapses (see **Fig. 1.1.b**) [16] generating high-speed jet of liquid towards a solid surface (in our case catalyst support materials [17].

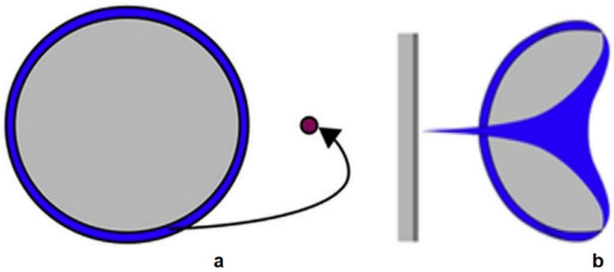

Fig. 1.1. Symmetrical (a) asymmetrical (b) bubble's collapse

In case of catalyst on support preparations, obviously the asymmetrical collapsing bubbles are of interest, the jets generated having high speed (~ 500 km/h) and introducing the liquids in all pores and crevasses of catalyst support [14], thus resulting a sound impregnation of it.

n-Butanol, a common product of the chemical industry, is a molecule with remarkable a transformation potential. It can also be obtained from renewable resources through fermentation, making it much more interesting for the chemical industry. This chapter focuses on the conversion of n-butanol to

butanal, one of the most useful transformations, on Cu catalysts. In the screening stage, various supports were used to generate cheap and innovative catalysts: TiO_2, CeO_2, ZrO_2, Al_2O_3, Celite22, MnO_2 and SiO_2. The main reaction products were monitored by gas chromatography to determine the best conversion and selectivity to the end product: butanal.

Butanal can be used as an intermediate to produce a wide range of chemicals: alcohols, plasticizers, polymers, and solvents, such as: polyvinyl butyral, MAK (methyl amyl ketone), n-butyric acid, 2-EH (2-ethylhexanol) or trimethylolpropane. It can be used as an important chemical for perfumery, flavors, antioxidants, pharmaceuticals, rubber accelerators, agrochemicals, and textile auxiliaries [18, 19]. Besides its easier preparation through the hydroformylation of propene, there is an interest in making it from naturally obtained n-butanol (from fermentation) due to the quality of the final products, required especially in the cosmetic industry where naturally occurring ingredients are highly regarded [20].

Butanal (n-butyraldehyde) is for the moment conventionally made by a well-known industrial process involving the conversion of propene by a hydroformylation reaction, over rhodium-phosphine catalysts (**Fig. 1.2.a**) [21-23]. Butyraldehyde could be also obtained by catalytic dehydrogenation of n-butanol (**Fig. 1.2.b**). n-Butanol could be available from synthetic pathway or from natural resources [24], usually via fermentation, making it a regenerable source for butyraldehyde.

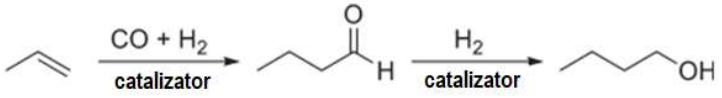

Fig. 1.2.a. Production of n-butanol by the OXO method

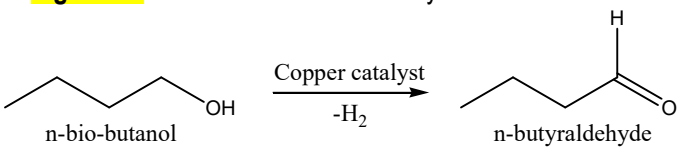

Fig. 1.2.b. Catalytic dehydrogenation of n-bio-butanol to butanal in the presence of copper catalysts

Next, it will be presented the influence of the support (TiO_2, CeO_2, ZrO_2, Al_2O_3, Celite22, MnO_2 and SiO_2) and the influence of the preparation method on the catalytic activity of the copper catalysts used for the dehydrogenation of n-butanol to butanal. Among these supported catalysts, three with the best performances were chosen, which were analyzed in detail and for which the performance comparison (selectivity and degree of conversion) is reported.

I.2. Laboratory experimental setup and working method

The prepared catalysts were submitted to tests. The test reactions were carried out in the laboratory installation (**Fig. 1.3**) in the downward vapor stream over a fixed bed catalytic reactor loaded with catalyst for testing. The catalyst was protected with a hydrogen stream at atmospheric pressure; the hydrogen also acted as carrier for reagents. The reactor was filled with catalyst mixed with an inert solid (glass powder 100 – 300 μm) at a mass ratio of 1:1 and arranged between two layers of glass wool within a tubular glass reactor (ø 10 x 170 mm). The vaporization layer and catalyst layer heights were kept constant at 70 mm and respectively 30 mm for all tested catalyst formulations. The reactor was mounted then inside a vertical tubular oven (2) and the catalyst was activated for 2 hours, at 400 ºC, in a hydrogen stream, at a flow rate of 10 cm3/min and gas hourly space velocity of 0.160 s-1. The temperature in the reactor was

maintained constant with a proportional-integral-derivative type temperature controller with an accuracy of ± 3ºC. The hydrogen flowrate was controlled with a mass flow controller.

The n-butanol was introduced in the reactor via a peristaltic pump (11) at a constant flow rate of 0.1 g/min, the liquid passing through a gas-liquid mixer where hydrogen was inserted. The n-butanol/hydrogen mixture then entered a preheater (3), filled with glass balls, acting as vaporizer. The preheater temperature was maintained constant throughout the experimental work at 325 ± 3 ºC. The reaction outcomes were condensed using two gas-liquid condensers cooled with ethylene glycol – water mixture having -20ºC temperature. A recipient with lateral tube for gases/vapors (10) for the collection of liquid samples was placed between the two condensers (9). The materials that remained in vapor phase after the first condenser entered the second condenser where additional liquid phase was condensed and collected in the same sample collector (10). The condensed liquid was collected and was weighed at 30 minutes intervals to be used in determining of the overall conversion of n-butanol and selectivities from the products. Non-condensable gases were sampled after the second condenser at 30 minutes intervals and the samples were analyzed in a gas chromatograph specially configured for the analysis of gas phase compounds (Buck Scientific 910).

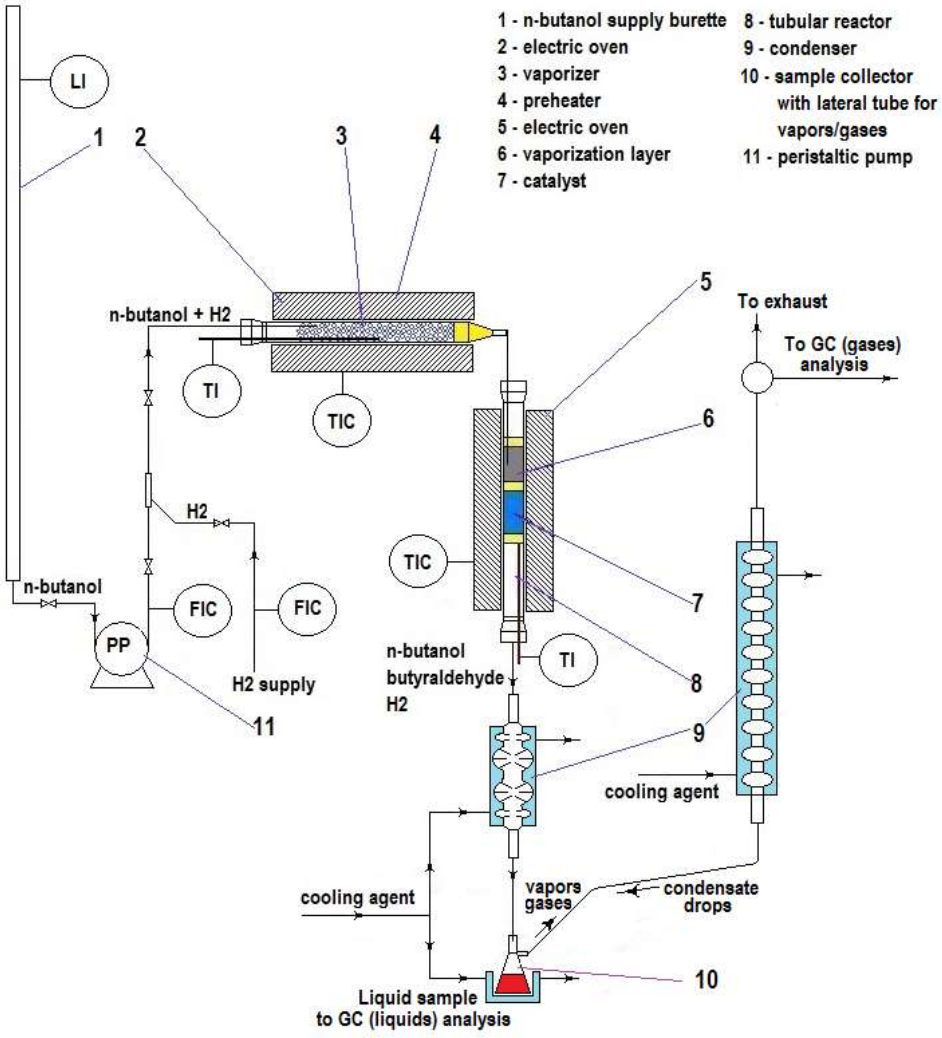

Fig. 1.3. Laboratory installation for testing of supported Cu catalysts (L – level, T – temperature, F – flow, I – indication, C – control, PP – peristaltic pump, GC – gas chromatograph)

In order to quantify the reaction products two offline gas chromatographs were used, one for the analysis of the liquid products (HP 6890 equipped with a flame ionization detector, internal calibration using iso-amyl alcohol as internal standard) and the other for the analysis of non-condensable products (Buck Scientific 910 equipped with a flame ionization detector and a thermal conductivity detector, calibrated for butene).

I.3. Catalysts Testing

The resulting gas and liquid phase from n-butanol catalytic reaction were passed through a condensation train, collected, and analyzed. The main compounds detected in the liquid phase were n-butyraldehyde, di-n-butyl ether and unreacted n-butanol (1,1 dibutoxy-butane, n-butyl-butanoate, 2-ethyl-hexanol and 2,4,6 tripropyl-1,3,5 trioxane being detected in very small quantities by GC-MS). In gas phase, the main detected products were: butenes and hydrogen.

The main reaction pathways of n-butanol under our conditions are the following (**Fig. 1.4.**):

- dehydration to produce butene;
- dehydrogenation to produce n-butyraldehyde;
- dehydration involving two n-butanol molecules to produce n-dibutyl ether.

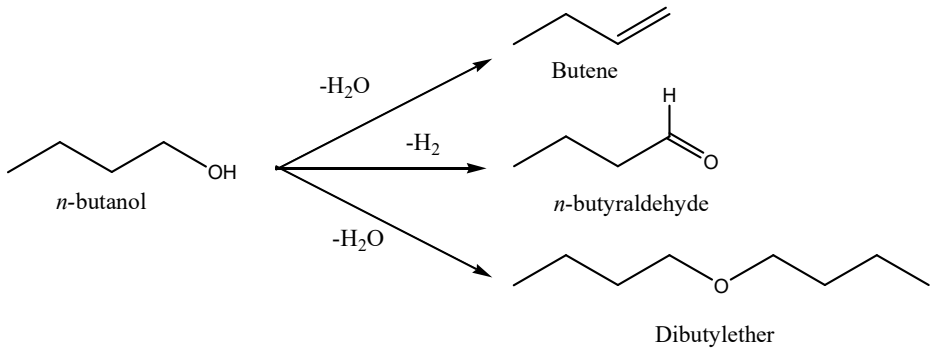

Fig. 1.4. Reaction pathways for the catalytic conversion of n-butanol to the main analyzed products

The catalysts shown in **Table 1.1.** were tested in the laboratory installation (Fig. 3) using the following working parameters: temperature of 300 ºC, 325 ºC and 350 ºC, corresponding to a gas hourly space velocity of 0.621, 0.648 and 0.675 s^{-1} respectively, time on stream of 1 hour for each test temperature, n-butanol flow rate of 0.1 g/min and hydrogen flow rate of 10 cm^3/min.

The following parameters were defined and monitored during the experimental activities, equations 1.1 and 1.2.:

$$\text{Conv} = \frac{m_2 - m_1}{m_2} \cdot 100 \qquad \text{Equation 1.1.}$$

$$Sel_1 = \frac{M_{W1}}{M_{W2}} \cdot \frac{m_3}{m_2 - m_1} \cdot 100 \qquad Sel_2 = \frac{M_{W1}}{M_{W3}} \cdot \frac{m_4}{m_2 - m_1} \cdot 100 \qquad \text{Equation 1.2.}$$

in which:

Conv – total n-butanol conversion,

Sel_1 – selectivity to n-butanal (main product),

Sel_2 – selectivity to n-dibutyl-ether (secondary product),

Sel_3 – selectivity to butene, $Sel_3 = 100 – (Sel_1 + Sel_2)$ (secondary product),
m_1 – mass of unreacted n-butanol,
m_2 – mass of n-butanol introduced into the system,
m_3 – mass of butanal obtained,
m_4 – mass of n-dibutyl ether obtained,
M_{w1} – molecular weight of n-butanol,
M_{w2} – molecular weight of butanal,
M_{w3} – molecular weight of n-dibutyl-ether

I.4. Catalysts preparation

The catalyst precursor amount (copper acetate or nitrate) was calculated to obtain the desired catalysts with a load of 10% copper. Catalysts with a load of 5% copper (M5 experiment) or with a load of 20% copper (M6 and S9 experiment) were also prepared in some cases as shown in Table 1. Two types of catalysts were prepared by wet impregnation with excess solution method: conventional and ultrasonic. In the case of the conventional preparation the precursor and the material used as support for the catalyst were introduced in distilled water and mechanically stirred at room temperature (2 hours, 400 rpm), followed by slow evaporation of the water on rotary evaporator under vacuum (12 hours, 90 rpm, 40 ºC with progressive raise of temperature up to 80 ºC in the last 4 hours), drying in the oven (12 hours, 110 ºC) and calcination of the catalyst (4 hours, 300 ºC or 350 ºC). In the case of ultrasonic preparation, the precursor and the material used as support for the catalyst preparation were introduced in liquid media (water: ammonia 10:1, 2-propanol: water 4:1 or glycerol: water 2:1). A reductive reagent was added and then ultrasonically irradiated at room temperature. For each reductive reagent used the sonication time was different. The temperature in the preparation vessel was maintained by external cooling with an ice bath.

The rest of the preparation steps are the same as for the case of conventional preparation. Four reductive reagents were used for preparation of catalysts using ultrasound: a) ascorbic acid, ultrasound irradiation using a Dr. Hielscher processor UP50H (15 minutes- continuous, 50% amplitude; 3 hours – pulse:5 s – ON, 1 s – OFF, 50% amplitude); b) 2-propanol, ultrasound irradiation using a Sonics Vibracell processor VCX750 (15 minutes - continuous, 30% amplitude; 6 hours – pulse: 5 sec ON, 2 sec OFF, 30% amplitude); c) 2-propanol:ammonia solution, using a Sonics Vibracell processor VCX750 (15 minutes - continuous, 30% amplitude; 3 hours – pulse: 5 sec ON, 2 sec OFF, 30% amplitude); and d) glycerol: water solution, using a Sonics Vibracell processor VCX750 (15 minutes - continuous, 30% amplitude; 3 hours – pulse: 2 sec ON, 2 sec OFF, 30% amplitude).

A mechanism of the interactions that occur in the presence of the ultrasound irradiation within the above-mentioned solution is described by the following reactions (R1 – R5):

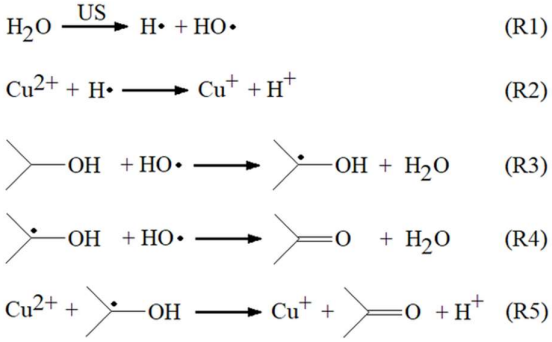

The reduction of Cu^{2+} to Cu^{+} (according to XRD data) is realized by the radical species produced from the decomposition of water in the presence of the ultrasound (R1) that produces H• and OH•. Both

species have potentials capable to transform Cu ions in solution ($E^0_{H\bullet}$ = − 2.4 V and $E^0_{OH\bullet}$ = + 1.9 V) [25]. Only H• atom is beneficial to the process for the Cu^{2+} reduction (R2). The other radical produced during the decomposition of water, HO•, has an oxidant character, and Cu^{+} reoxidation is avoided by adding isopropyl alcohol to consume it (R3-R4). Reaction (R5) contributes also to the reduction of Cu^{2+} as a step to the transformation of isopropyl alcohol into acetone [25].

The temperature in the preparation vessel was the room temperature.

In all cases, before testing the catalytic activity the catalysts were reduced to metallic form (which is the active form) in the installation used for experimental work for 2 hours, at 400 ºC, in a hydrogen stream, at a flow rate of 10 cm^3/min and gas hourly space velocity of 0.160 s^{-1}. The catalysts prepared according to the above-described procedures are presented in **Table 1.1**.

Table 1.1. Catalysts prepared and tested in the heterogeneous gas/solid phase reaction of n-butanol to butanal

Catalyst	Experiment code	Support	Precursor	Metal load	Preparation method	Solvent
Cu/TiO_2	T1	TiO_2	$Cu(CH_3COO)_2$	10%	conventional	distilled H_2O
Cu/CeO_2	Ce1	CeO_2				
Cu/ZrO_2	Z1	ZrO_2				
Cu/Al_2O_3	A3	Al_2O_3	$Cu(CH_3COO)_2$			
	A3R		$Cu(NO_3)_2$			
Cu/SiO_2	C2R	Celite22	$Cu(CH_3COO)_2$			
	C3		$Cu(NO_3)_2$			
Cu/MnO_2	M2R	MnO_2	$Cu(CH_3COO)_2$			
	M2R1					
	M4		$Cu(NO_3)_2$	5%		
	M5			10%		
	M6			20%		
	M7		$Cu(CH_3COO)_2$	10%		
Cu/SiO_2	S3R	SiO_2				
	S3R1					
	S3R2					
	S5		$Cu(NO_3)_2$			
	S6		$Cu(CH_3COO)_2$		US – NH_3	distilled H_2O + NH_3
	S7				US	2-propanol: H_2O 4:1
	S8					Glycerol: H_2O 2:1
	S9			20%		2-propanol: H_2O 4:1

US – ultrasound impregnation.

I.5. Determination of global copper content of the catalysts by titration

The copper concentration of the catalysts was tested by a chemical method with insignificant deviations from the proposed values.

A quantity of unreduced catalyst (0.5 g) was reacted with an aqueous solution of acetic acid (50%). After catalyst disintegration with acetic acid, the pH of the solution containing copper acetate was verified with pH paper. Then the solution containing the cation was titrated with a solution of sodium thiosulfate (0.01 M) in presence of potassium iodide and sulfuric acid (0.1 N) until the color turned to light yellow. After this first step potassium thiocyanide (0.1 mol/L) and starch were added, and the titration continued until the solution turned colorless [16].

The results were determined using the calibration curve described in **equation 1.3.**

$$V_{Na2S2O3} = 944.39024x + 0.3439 \qquad \text{Equation 1.3.}$$

Were,

x – quantity of Cu^{2+} in solution, mol/L;

$V_{Na2S2O3}$– volume of $Na_2S_2O_3$ solution (0.01 M), used for titration;

944.39024 – slope of the line described in **equation 1.3**.;

0.3439 – interception of the V_{Na2SO3} axis.

RESULTS AND DISCUSSION

I.6. Catalytic activity for all catalysts tested throughout the screening

The catalysts shown in the **Table 1.1.** were tested in gas/solid phase dehydrogenation reaction of n-butanol to n-butyraldehyde at three test temperatures (300 ºC, 325 ºC and 350 ºC, corresponding to a gas hourly space velocity of 0.621, 0.648 and 0.675 s^{-1} respectively and time on stream of 1 hour for each test temperature).

I.6.1. Results of the catalysts screening

The catalysts shown in **Table 1.1.**, were tested in the laboratory installation (Fig. 1.3.) using the following working parameters: temperature of 300 ºC, 325 ºC and 350 ºC, corresponding to a gas hourly space velocity of 0.621, 0.648 and 0.675 s-1 respectively, time on stream of 1 hour for each test temperature, n-butanol flow rate of 0.1 g/min and hydrogen flow rate of 10 cm3/min. The results are summarized in **Figs. 1.5** and **1.6**, Ox axis being the experiment code and Oy axis the parameters Conv, Sel1, Sel2 described in **equations 1.2** and **1.3.**

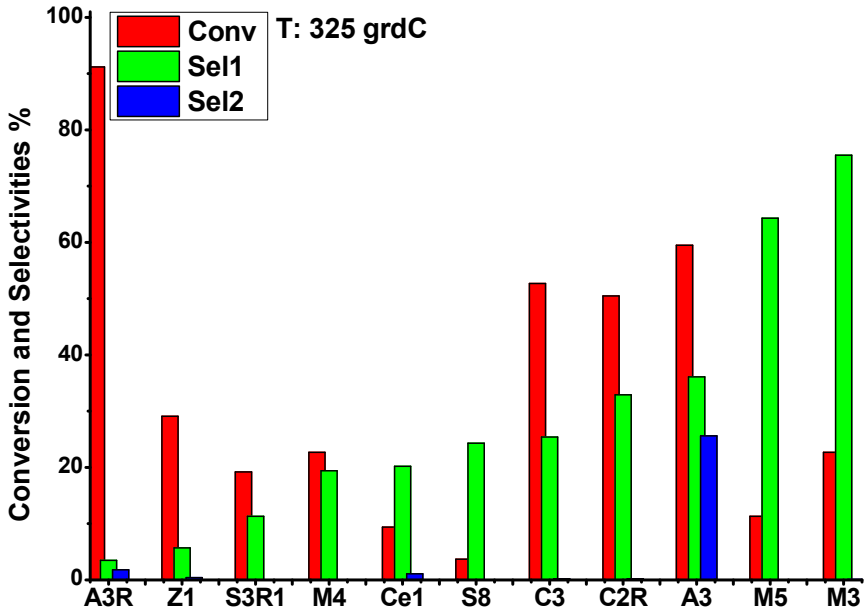

Fig. 1.5. The results of the catalyst screening presented in **Table 1.1.** to temperature of 325 °C (catalysts with low selectivity to butanal)

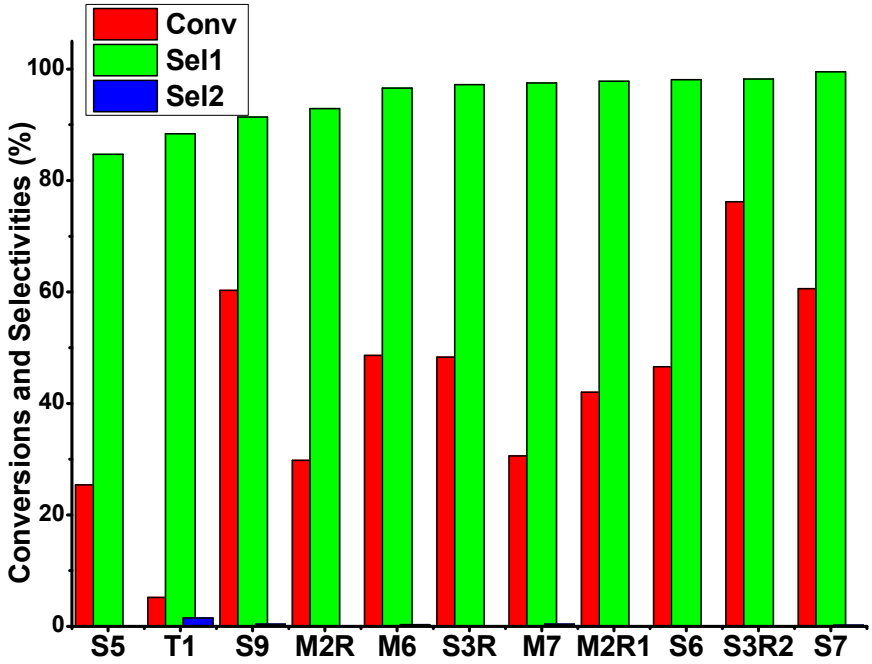

Fig. 1.6. The results of the catalyst screening presented in **Table 1.1.** to temperature of 325 °C (catalysts with high selectivity to butanal)

After this first trial of catalysts, it is clearly shown that those selected in **Fig. 1.6.** are the most promising catalysts from both overall conversion of n-butanol and selectivity to n-butyraldehyde (except T1 catalyst: low conversion, high selectivity).

The analysis of data presented in **Fig. 1.5. and 1.6.** reveals the following aspects:

a) Cu/SiO_2 type catalysts (S5, S9, S3R, S6 and S3R2 experiments from **Fig. 1.6.**) exhibit very good selectivity to butyraldehyde (over 90%), with very little amounts of undesirable compounds;

b) the catalysts deposited on Al_2O_3 support (A3 and A3R experiments from **Fig. 1.5.**) have the highest conversion of n-butanol, but rather low selectivity to butyraldehyde (below 40%). However, a special case should be noted for A3R experiment in which butene selectivity was nearly 95% for n-butanol conversion of 91.2%, over a catalyst prepared from $Cu(NO_3)_2 \cdot 3H2O$ precursor. This is not a desired reaction but could be an efficient potential method to produce butene from green n-butanol if it is the target product;
c) Cu/MnO_2 type catalysts (M5, M3, M2R, M6, M7 and M2R1 experiments) show rather good selectivities to butyraldehyde (more than 60%), but low conversion of n-butanol;
d) in case of Cu/MnO_2 type catalysts, the metal loading of the support influences the catalytic activity which increases as the percentage of metal deposited on support increases: 5%, 10% and 20% (comparison between M5, M3 and M6 experiments). It is noteworthy that with conversion the selectivity increases, both due to the increase in the catalyst content of Cu as well as due to the increase in temperature over the studied range: 300 – 350 ºC;
e) in the presence of the catalysts obtained in presence of US (S6, S7 and S9 experiments) the selectivities to butyraldehyde obtained are somewhat higher than those obtained in the presence of the conventional catalyst (S3R2 experiment).
In all considered cases, besides butyraldehyde, the quantities of other products are present in traces. The reduction of $Cu(CH_3COO)_2$ in the presence of NH_3 and US (S6 experiment) does not lead to better results than those obtained in the presence of catalysts prepared only in the presence of the US.
f) the catalytic activity of catalysts prepared from precursor $Cu(NO_3)_2 \cdot 3H_2O$ is significantly lower than in the case of the catalysts prepared from precursor $Cu(CH_3COO)_2 \cdot H_2O$ (experiment S5 compared to S3R);

Because the catalysts **S3R2** – conventional preparation and **S7** and **S9** – ultrasonic preparation had the best results of catalytic activity and selectivity to butanal, they are further investigated and characterized in detail using techniques such as: XRD – X-ray Diffraction, EDX – Energy Dispersive Spectroscopy, Nitrogen Adsorption-Desorption Isotherms, TGA/DTG – Thermogravimetric Analysis, TPD-Pyridine – Pyridine Thermal Desorption, FTIR - Fourier Transform Infrared Spectroscopy and SEM - Scanning Electron Microscopy.

Also, for the convenience of working with these catalysts, I will switch to a new coding which is more suitable to the declared purpose of explaining the catalytic activity results, the selectivity to butanal and the selectivities to secondary products: **S3R2 = CONV**; **S7 = US10**; **S9 = US20**.

Thus, the tabular representation of these catalysts, together with the new coding, could be found in **Table 1.2**.

Table 1.2. Catalysts selected for further investigation/characterization

Catalyst	Exp. Code	Support	Precursor	Metal load	Preparation method	Solvent
Cu/SiO_2	CONV	SiO_2	$Cu(CH_3COO)_2$	10%	Conventional	2-propanol: H_2O 4:1
	US10				US	
	US20			20%		

US - ultrasound

I.7. Determination of the Cu load of the selected catalysts

The Cu load of the selected catalysts CONV, US10 and US20 was determined using two methods:
(a) titration of Cu by classical chemical analysis;
(b) EDX analyses.
The results of determining the Cu content of the catalysts are presented in **Table 1.3**.

Tabel 1.3. Determination of Cu content of selected catalysts

Catalyst	Exp. Code	Preparation method	Cu load method (a) (%)	Cu load EDX (b) (%) *
Cu/SiO_2	CONV	conv.	7.91	10.9 ± 0.62
	US10	US	7.84	8.7 ± 0.41
	US20		15.99	12.9 ± 0.76

* Mediated values of five determinations at different areas

It must be stressed out that the determination of Cu by method (a) is a global determination of Cu from the pores of the support as well as from the surface of the support. On the other hand, the determination by method (b) is a partial determination only of Cu deposited on the surface of the support. The difference between the Cu load determined by EDX (b) and titration (a) could be explained in the case of catalysts with the same Cu load (approx. 8% for CONV and US10) by a more uniform Cu distribution into the pores of silica support achieved through US impregnation. In catalyst US20, the Cu distribution on the surface is uneven, and as a result, the differences will also be significant.

I.8. Determination of textural parameters of catalysts

The N_2 adsorption–desorption isotherms for the three catalysts were recorded at liquid nitrogen.

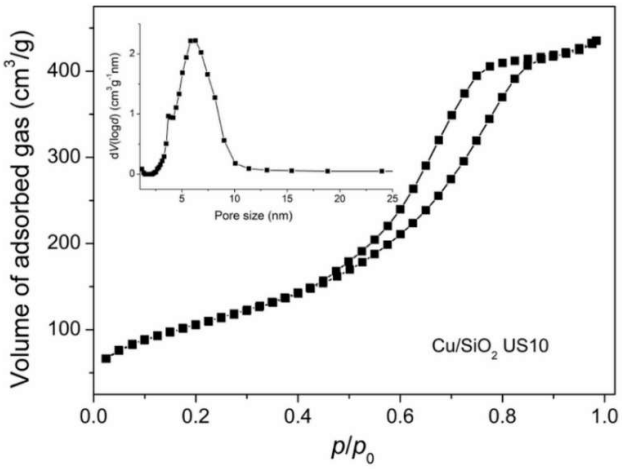

Fig. 1.7. N_2 adsorption-desorption isotherm of US10 catalyst. Inset the corresponding pore size distribution curve

The N_2 adsorption–desorption isotherms for CONV and US20 catalysts are almost identical to those for catalyst US10 which is shown in **Fig. 1.7**. The shape of these isotherms is type IV (a) according to IUPAC,

with H2-type hysteresis due to capillary condensation of nitrogen. The textural parameters, specific surface area determined with BET method, S_{BET}, average pore diameter computed according to BJH theory from the desorption part of isotherm, d_{BJH}, total volume of pores measured up to relative pressure of 0.99, V_{tp}, and mesopores volume with a lower diameter of 10 nm, V_p (measured in the relative pressure range 0.17–0.8) are listed in **Table 1.4**.

Table 1.4. Textural parameters determined from N_2 adsorption-desorption isotherms for selected catalysts

Catalyst	Exp. Code	Prep. method	S_{BET} (m^2/g)	d_{BJH} (nm)	V_{tp} (cm^3/g)	V_p (cm^3/g) (d<10 nm)	Blocked pores V_{PT} (%)
SiO_2 (support)			447	5.83	0.80		0
Cu/SiO_2	CONV	conv.	348	5.82	0.78	0.68	2.5
	US10	US	381	5.82	0.71	0.67	11.25
	US20		325	5.81	0.61	0.57	23.75

V_{PT}— percent of blocked pores

The pore diameter for the support and the three catalysts is virtually identical and confirms the observations from the adsorption isotherms, but the total pore volume decreases in the following order: Support > CONV > US10 > US20. The reduction of S_{BET} in the order described above suggests that crystallites of copper are also present inside the support's pores, not only on its surface. In some cases when the diameter of certain pores is less than a limit value, these crystallites can block these pores.

I.9. TGA and TPD – Pyridine desorption

The three catalysts, both in the simple form (00) and in the pyridine exposed one (Py), were subjected to TGA and the graphs are presented in **Fig. 1.8.**

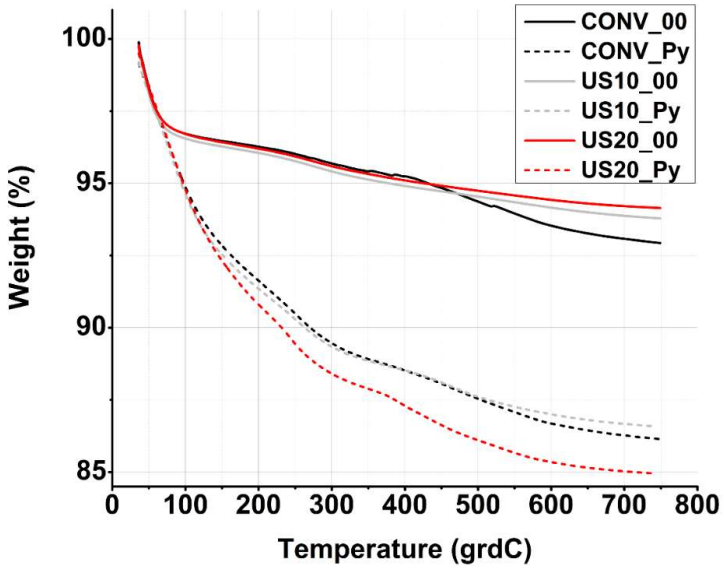

Fig. 1.8. TGA for simple catalysts (00) and pyridine-exposed catalysts (Py)

The weight loss for catalysts in simple form (00), from **Fig. 1.8**, is quite small and is in the range of 5.85 to 7.06% at 750 °C. For the catalysts exposed to pyridine (Py), from the same figure, the weight loss

is in the range of 13.42 to 15.05% at the same temperature of 750 °C. This small weight loss of the catalysts in simple form (00) could be explained by the fact that immediately after preparation the catalysts were calcined at 350 °C for 4 h.

Further, from the TGA data, presented in **Fig. 1.8**, the acid–base properties of the catalysts were evaluated.

These acid-base properties were characterized by TPD-Py, previously described in literature [26, 27]. Through this technique, depending on the weight loss due to the desorption of pyridine from the acidic sites of a catalyst, the total surface acidity is determined using equation 1.4 [28]:

$$\Psi = \frac{N_{Py}\, N_A}{m_{CAT} S_{BET}} \qquad \text{Equation 1.4}$$

Where:

Ψ – acidity of the catalyst (sites/m^2_{CAT});

N_{Py} – pyridine desorbed from catalyst as a difference from TGA curve for (00) catalyst and TGA curve for (Py) catalyst (moles);

N_A – Avogadro's number (sites/mol);

m_{CAT} –catalyst sample mass (g);

S_{BET} – catalyst specific surface area determined with BET method (m^2/g).

Data obtained from the TPD-Py of exposed catalysts are calculated using Equation 1.4 and are represented in **Fig. 1.9**.

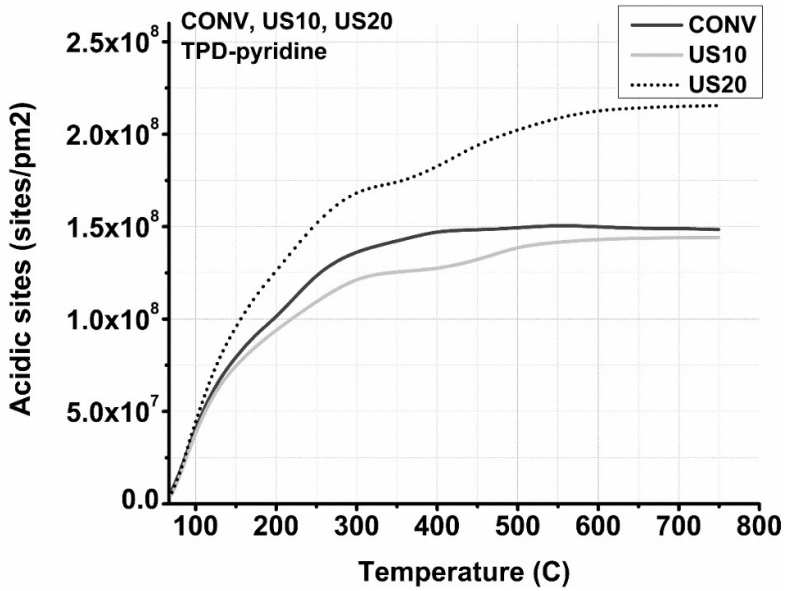

Fig. 1.9. TPD — pyridine — total acidic sites and strength of these acid sites for the CONV, US10 and US20 catalysts as a function of temperature desorption of the absorbed pyridine (sites/picometer^2)

As can be observed in **Fig. 1.9**, the total number of acidic sites for the three studied catalysts increases in the following order: US10 < CONV < US20. Total surface acidity, Ψ, is a sum of Lewis and Brönsted acid sites (Ψ = L + B). It is also possible to segregate acidic sites depending on the temperature at which Py is absorbed on them. Thus, for temperatures below 200 °C there are weak acid sites, for temperatures between 200 and 400 °C there are medium-acid sites, and for Py desorption temperatures

above 400 °C there are strong-acid sites [29]. The ascending order of the number of weak-acid sites is: US10 ≤ CONV < US20. The same ascending order is maintained for strong-acid sites.

I.10. FTIR

Data in **Fig. 1.10.** represent the FTIR spectra for Py adsorbed on acidic centers of CONV, US10 and US20 catalysts in the range 400 – 1400 cm^{-1}.

From the FTIR spectra for Py adsorbed on the acid centers of the catalysts, represented in **Fig. 1.10**, the segregation of the Lewis and Brönsted acid sites can be detected [29].

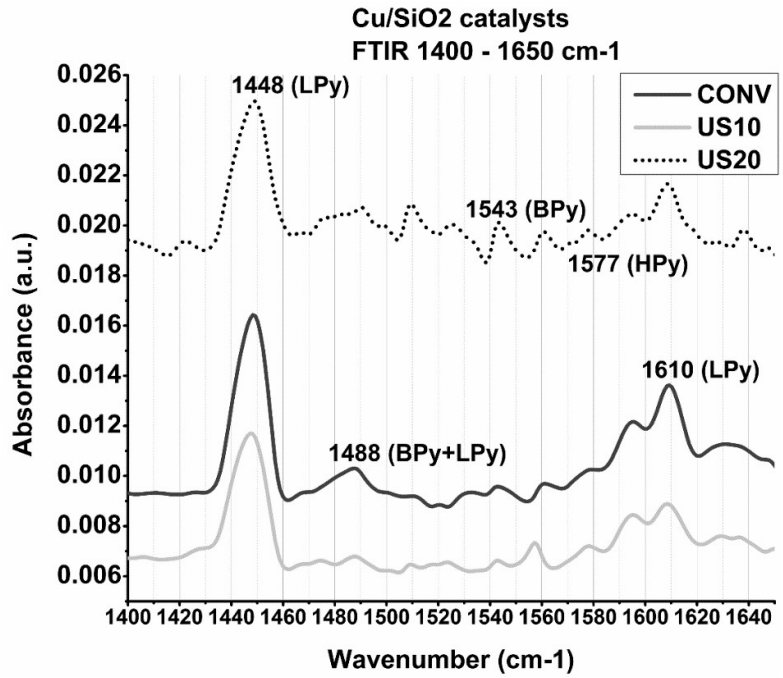

Fig. 1.10. FTIR spectra for Py adsorbed on Cu/SiO_2 catalysts: CONV, US10 and US20 in the 1400 – 1650 cm^{-1} range (B – Brönsted, L – Lewis)

The FTIR spectra of pyridine chemisorbed on SiO_2 are very simple: only two strong bands at 1448 cm^{-1} (ν_{19b}) and 1595 cm^{-1} (ν_{8a}) [30].

The band peaks characteristic of the Lewis and Brönsted acid sites appearing in the FTIR spectra of (Py) catalysts in **Fig. 1.10.** can be seen at the following wavenumbers [29, 31]:

(a) **1448** cm^{-1} – ν_{19b} – assigned to Lewis acid sites of SiO_2 (SiO_2-L-Py) [30], for which the largest area is found in the case of CONV and the smallest for US10;

(b) 1488 cm^{-1} – ν_{19a} – characteristic for pyridine adsorbed on Lewis acid sites (L-Py) together with Brönsted acid sites (B-Py), the increasing order of peak areas being US10 < CONV < US20;

(c) 1543 cm^{-1}, the peak area being proportional to the concentration of Brönsted acid sites (B-Py) with increasing values in the order of US10 < CONV < US20. These Brönsted acid sites may be of the type: –O–Si–O–H+, but they can also be protons generated by reducing Cu^{+} and Cu^{2+} in hydrogen medium according to the following reactions: $2Cu^{+} + H_2$ ---> $2Cu^{0} + 2H^{+}$ and $Cu^{2+} + H_2$ ---> $Cu^{0} + 2H^{+}$. During the pretreatment of Cu containing samples in vacuum prior to pyridine sorption measured by FTIR, and under assumption of the moisture existence at least in residual content, the occurrence of the reaction $Cu^{2+} + H_2O$ ---> $CuOH^{+} + H^{+}$ is not excluded [32];

(d) 1577 cm^{-1} – v_{8b} - considered specific for acidic Brönsted H-Py sites for which the largest peak area is US20 (could be protons generated by reducing copper ions in the hydrogen atmosphere);

(e) **1595** cm^{-1} – v_{8a} – Py molecules are coordinated to Lewis sites of SiO_2 (SiO_2-L-Py) [30, 33];

(f) 1610 cm^{-1} – characteristic band of Py bound to Lewis acid sites for which the smallest area is US10, and the largest area belongs to CONV.

Also, the vibrations mentioned at points (a), (b), (d) and (e) are the Py ring-breathing vibrations (vCCN) [27] of irreversible absorbed Py.

I.11. SEM Analysis

SEM analysis revealed the shape of the metallic particles, how these aggregated and their distribution on the surface of the support.

Cu/SiO_2 conv.

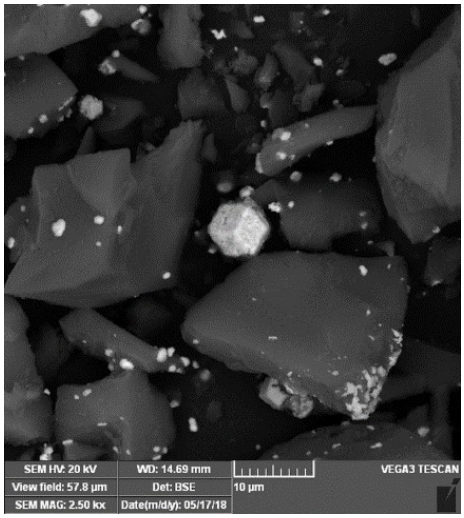

Fig. 1.11. SEM Image (2.50 kx) - CONV

Cu/SiO_2 10% - US

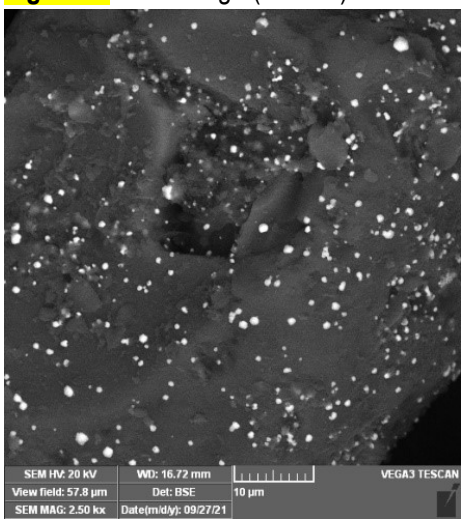

Fig. 1.12. SEM Image (2.50 kx) – US10

Cu/SiO_2 20% - US

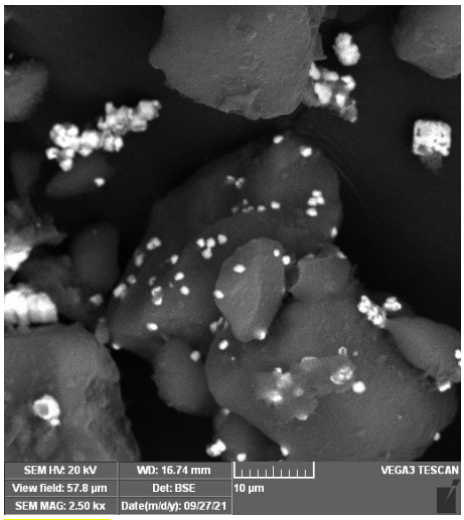

Fig. 1.13. SEM Image (2.50 kx) – US20

Table 1.5. Copper particle analysis on support surface

Catalyst	Particle size (SEM), µm			Crystallite size (XRD), nm
	min	Max	mean	
CONV	0.61	2.54	1.15±0.52	41
US10	0.44	1.16	0.88±0.20	44
US20	1.05	1.89	1.48±0.28	47

Table 1.5. shows both the dimensions of the crystallites (obtained from the XRD analysis [34-36]) and the dimensions of the metal particles (determined using SEM analysis). The size of the crystallites in catalysts with the same Cu load (%wt.) is higher for US10 compared to CONV due to a much more uniform impregnation in the presence of US. This more uniform impregnation could produce larger crystallites in the drying and calcination stages of the catalysts. On the other hand, the metal particle size (SEM) for US10 is slightly smaller than in the case of CONV because the impregnation of the support is much more uniform in the case of US-assisted preparation. The explanation makes sense because ultrasound causes a deeper impregnation of the support (including pores — in **Table 1.4.** the volume of blocked pores increases in this order: CONV < US10). In **Figs. 1.11 – 1.13.** there are some representative images of Cu particles for the three studied catalysts. **Figure 1.11.**, corresponding to catalyst CONV, shows that some of the Cu particles present on the surface of the support are aggregated in some sort of cubic aggregates of 4–5 µm. These aggregates could be formed during the preparation procedure but also during the procedure of reducing copper ions to metallic copper [32]. Even if the Cu load on the external coat of the CONV catalyst is higher than in the case of catalyst US10, because of the Cu aggregates, the percentage of the acid centers of SiO2 (on which intermolecular and intramolecular dehydration reactions occur) [37] has a bigger value compared to the metallic centers of Cu (that promotes the dehydrogenation reaction) [38]. On the other hand, the US10 catalyst has a better coverage of the support surface by Cu particles (**Fig. 1.12.**) that have a more uniform dimension. Based on the SEM investigation for the catalyst US20 one can observe that the surface of this catalyst presents large aggregates of Cu particles (**Fig. 1.13.**), which are unevenly distributed on the surface of the support. The discussion regarding the appearance of large Cu particle aggregates is identical/similar to the one of the CONV catalyst.

I.12. Effect of the catalyst synthesis method on the dehydrogenation of butanol (CONV, US10 and US20) – resuming at a more advanced level

The catalytic activity of the prepared catalysts: CONV (conventional impregnation), US10 and US20 (impregnation in the presence of US) was determined in the laboratory installation described in **Fig. 1.3.**. The conversion of n-butanol (Conv) and the selectivity to butanal (Sel1), di-n-butyl ether (Sel2) and butene (Sel3) were calculated as a media of three different determinations and are represented in **Fig. 1.14.** for each catalyst.

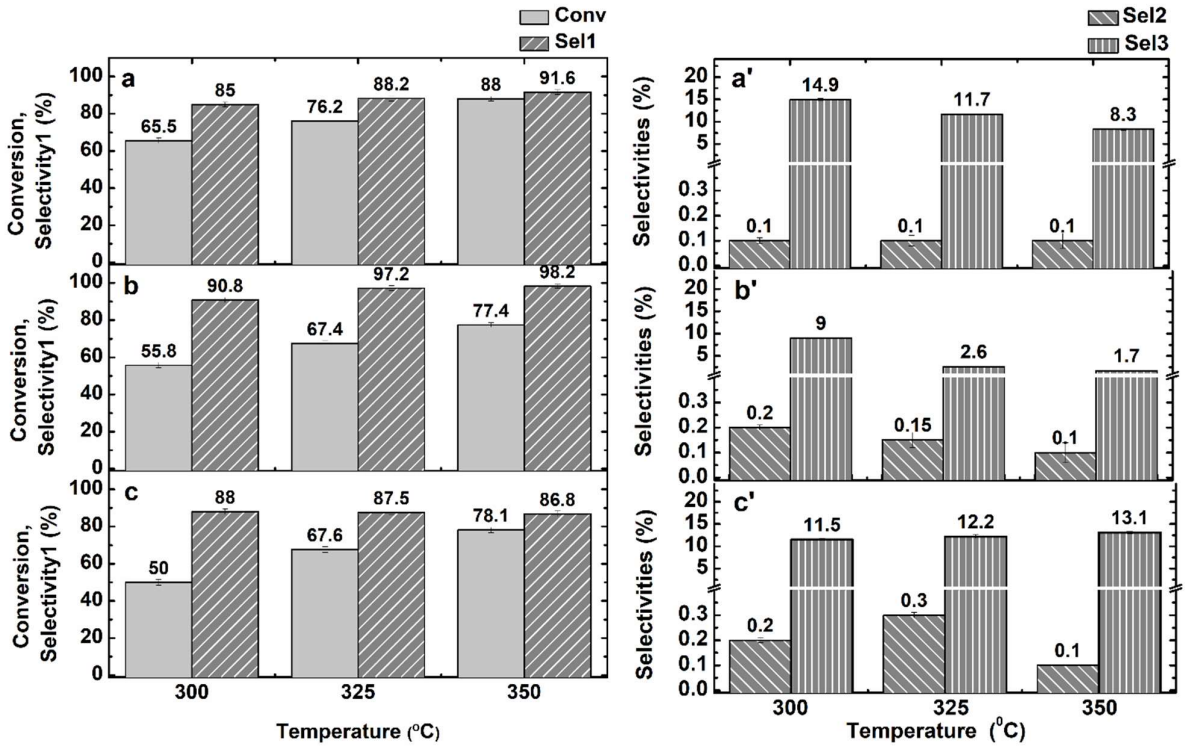

Fig. 1.14. Influence of the preparation method on the catalytic activity of the catalyst: (a) conventional impregnation (exp. CONV), (B) US impregnation, Cu10% (exp. US10), (C) US impregnation, Cu20% (exp. US20)

The analysis of catalyst activity data in **Fig. 1.14.a** shows that in the presence of the conventionally prepared catalyst, the conversion of butanol (Conv) had the highest value of all the values obtained for the three catalysts studied. Conversion of butanol increases with temperature (Conv: from 66.5% at 300 °C to 88% at 350 °C) and so does the selectivity to butanal (Sel1: from 85% at 300 °C to 91.6% at 350 °C). The selectivity to butene (Sel3) in **Fig.1.14.a'** decreases with temperature from 14.9% at 300 °C to 8.3% at 350 °C. The selectivity to n-dibutyl ether (Sel2) in **Fig. 1.14.a'** is constant at 0.1%. These facts analyzed together with SEM (**Fig. 1.11.**) and BJH (**Table 1.4.** – textural parameters) satisfactorily explain the catalytic activity of this catalyst.

For the catalysts prepared in the presence of ultrasound (**Fig. 1.14.b** and **1.14.c**) [6, 39], the conversion of n-butanol is slightly lower than the one of the conventionally obtained catalyst, but the selectivity to butanal increases, especially when the copper content of the catalyst is only 10%. In the presence of catalysts US10 and US20, very small amounts of dibutyl ether are also obtained. As a comparison between the catalysts prepared in presence of ultrasound, US10 and US20, the most favorable values of selectivity to butanal are recorded for US10 catalyst. This may be explained by the uniform

distribution of metal particles on support as shown in the SEM analysis (**Fig. 1.12.**). The better results in terms of selectivity to butanal, 98.2% at 350 °C, and selectivity to butene, 1.7% at 350 °C, are obtained for US10 catalyst (**Fig. 1.14.b/b'**) that has a better coverage of the catalyst surface with Cu crystallites (**Fig. 1.12.**) because of their more uniform dimension.

Dehydration reactions usually occur on Brönsted acid sites (B-Py and H-Py in **Fig. 1.10.** - FTIR). Dehydration to butene occurs on strong-acid Brönsted sites, while dehydration reaction to dibutyl ether occurs on weak-acid Brönsted sites [37]. TPD-pyridine data in **Fig. 1.9.** (acidity) describes the total surface acidity Ψ = Lewis acidity (L) + Brönsted acidity (B) of the catalysts and the segregation of acid sites into weak, medium and strong acid. FTIR data provide even more detailed data about Brönsted acid sites. The peak area at 1543 cm^{-1} (B-Py), 1488 cm^{-1} (B-Py + L-Py) and 1577 cm^{-1} (H-Py) from **Fig. 1.10.** gives information that allows the ordering of the catalysts according to their number of Brönsted acid sites. Considering the previous data, the three catalysts are ordered as a function of Bronsted weak-acid strength, as follows: US10 ≤ CONV < US20. Thus, the data on the acid strength of Bronsted weak-acid sites can explain the values of the selectivity to dibutyl ether (Sel2) from **Fig. 1.14.a', b' and c'**.

On the other hand, the strong-acid sites strength, from **Fig. 1.9.** (acidity), of the catalysts increases in this order: US10 < CONV < < US20. To this statement, the data from Fig. 6 are added as they describe the number of Brönsted acid sites, which for the form B-Py (1543 cm^{-1}) increase in this way: US10 < CONV < US20 and for the form H-Py increase in this order: US10 ≤ CONV < US20. On a first analysis of the three parameters listed above, it is clear that US10 has the lowest number of Brönsted strong-acid sites which is consistent with the value of the selectivity to butene (Sel3) from **Fig. 1.14.b'**. The discussion remains open to explain the Sel3 values for CONV and US20 catalysts. However, Ψ = L + B, and L, the number of Lewis acid sites, increases from US20 to CONV (**Fig. 1.10.**, peaks at: 1448 cm^{-1}, 1596 cm^{-1} and 1610 cm^{-1}). Thus, it can be concluded that, in fact, the amount of Bronsted strong-acid sites for the two catalysts does not differ too much. But the data in **Fig. 1.10.** (1543 cm^{-1} and 1577 cm^{-1}) impose that the number of Brönsted strong-acid sites be slightly higher in the case of US20. This explains why the values of selectivity to butene in **Fig. 1.14.a'** and **c'** are not very different and why the Sel3 for US20 still takes higher values than those for CONV.

Metallic centers of copper promote the dehydrogenation reaction [38, 40]. Considering the data stated in the previous paragraphs, there are many parameters that influence the butanal selectivity of the three catalysts analyzed: (a) copper load on the support surface (Cu_{EDX}: US10 ≤ CONV < US20), (b) the actual size of the particles observed on the support surface, determined statistically by SEM, US10 < CONV < US20 (**Table 1.5.**) and finally (c), the uniformity with which the copper is distributed on the support surface (copper uniformity, U_{Cu}). A more uniform coverage of the support surface by active phase exposes to the diffusion of n-butanol molecules a smaller surface of the carrier, SiO_2. This has the effect of decreasing the total acidity of the catalyst. As a result, the dehydrogenation reaction becomes predominant.

SEM images of the catalyst surface of CONV in **Fig. 1.11.** indicate the presence of some metal particles grouped in cubic aggregates with an approximate dimension of 4–5 μm. Also, the SEM images for US20 surface in **Fig. 1.13.** prove the existence of large metal particle aggregates that are unevenly distributed on the support surface. From the SEM image in **Fig. 1.13.** and the other SEM images it is observed that US10 is the only catalyst on whose surface there is a uniform distribution of metal particles that have similar dimensions. Moreover, although the metal loading (determined by EDX) on the surface of the CONV catalyst is higher than the one detected in the case of US10 catalyst, the existence of metal agglomerates on the CONV surface results in the percentage of Brönsted acid sites being higher than the one of the active metallic sites. In addition, global determination of copper for US20 catalyst shows a value

almost double in size than the one for the catalysts CONV and US10 (which have approximately equal values of the total amount of copper deposited **Table 1.3.** -- Cu concentrations, approx. 7.9% compared to 15.99% for US20). This fact, analyzed at the same time with the concentration of copper on the surface of the support (EDX measured), together with the percentage of blocked pores (V_{PT}, **Table 1.4.**), demonstrates that: (a) a small amount of copper is embedded inside the silica pores (thus becoming inactive) of US10; and (b) a significant amount of Cu is blocked in the pores of US20 catalyst. Therefore, the data listed above quantify the Cu uniformity, U_{Cu}, mentioned at point (c) in which U_{Cu} increases in this order: CONV < US20 < US10.

The weighted average of (a) - (c) parameters together with the selectivity to by-products results in the selectivity to butanal of the three catalysts increasing as follows: US20 < CONV < US10 order that is in accordance with the data represented in **Fig. 1.14**. Catalytic activity depends on parameters such as: (a) the concentration of copper on the support surface (particle diameter and particle number), (b) the uniformity of copper distribution, U_{Cu}, defined above, which influences the ratio between the acidic sites of the support and the active metal sites. The number of Brönsted acid sites decreases in this order: US20 > CONV > US10. Thus, there is a decrease in the intensity with which the side reactions take place. As a result, the values of selectivity to by-products: butene and dibutyl ether also decrease. The catalytic activity of US10 decreases slightly compared to that of CONV because the Cu content deposited on the surface of the catalyst decreases from 10.9% to 8.7% (EDX, **Table 1.3.**). Total surface acidity increases and implicitly the Brönsted acidity increases from US10 catalyst to US20 catalyst. As such, the intensity of side reactions expressed by selectivity to by-products also increases. The catalytic activity of US20 decreases due to the smaller specific surface area (S_{BET}, **Table 1.4.**) and the higher volume of blocked pores in the case of US20 catalyst (V_{PT}, **Table 1.4.**, 11.25% for US10 and 23.75% for US20). Therefore, the catalytic activity of the three catalysts evolves as follows: CONV > US10 ≈ US20, which satisfactorily explains the experimental data for the conversion of n-butanol and the selectivities in by-products in **Fig. 1.14.** catalytic activity.

Two types of Cu/SiO_2 catalysts were prepared through the wet impregnation method performed conventionally or in the presence of ultrasound. The catalysts were tested in the process of n-butanol dehydrogenation to butanal. The direct comparison between physicochemical properties and catalytic performance led to the conclusion that high selectivity to butanal could be related to: (a) a greater uniformity of the surface coverage of the support by active phase, (b) a more uniform dimension of Cu nanoparticles observed in the case of US10 catalyst and (c) a lower acidity of catalyst. Thus, previous experimental data demonstrate that ultrasound-assisted preparation can be an efficient and inexpensive method for obtaining high-performance catalysts.

Chapter II.

Catalytic activity of some nickel catalysts tested for production of synthesis gas by methane reforming with carbon dioxide. Conventional and Microwave heating

OBJECTIVES

O3. Preparing some nickel catalysts on alumina support through co-precipitation and sequential precipitation;

O4. Determining the overtime stability of the catalysts prepared by endurance tests in the dry reforming reaction of CH_4 with CO_2;

O5. Intensifying the catalytic activity by using microwaves

II.1. Introduction

Dry and wet reforming of methane with carbon dioxide is a useful method when it comes to solving the big environmental issues our planet faces. Wet reforming of methane with carbon dioxide is a process similar to dry reforming, except that superheated steam is added to the two established reactants. The suite of reactions for the dry reforming of methane with carbon dioxide is therefore augmented by the reactions of water with active species derived from methane, carbon dioxide, carbon and carbon monoxide [41-43].
The increase in carbon dioxide emissions caused mainly by the large combustion plants, the cement plants, and the intensive use of the means of transportation has already become a problem that is viewed as critical by a large part of the European and world's scientific community [44-49].

Likewise, the methane emissions generated by the decomposition of methane clathrates (retained so far by the tundra regolith) due to global warming, but also the huge number of animals used as food bioprocessors (which emit biogas [50, 51] as a result of digestion processes), cause problems since methane has a potential to increase the greenhouse effect 21 times higher than carbon dioxide [52]. Biogas could be upgraded to biomethane, which becomes a valuable fuel in the context of REPowerEU and the Biomethane Action Plan of the European Commission.

The methods of (a) capturing carbon dioxide directly from the source (so far only from cement plants) or (b) the use of methane-rich natural gas (the new natural gas exploitation perimeters on the continental platform of the Black Sea should also be taken into account here: Ana and Doina which have recently delivered natural gas to the National Transport System) but also biogas/landfill gas/biomethane [53] produced as a by-product of installations that reduce the organic load values of some aqueous industrial effluents are imposed by environmental legislation in the European Union and have recently gained momentum.

When using carbon dioxide and methane in the DRM (dry methane reforming) process [54-70] or the CSDRM one (Dry and wet reforming, with steam, of CH_4 with CO_2) [41-43, 71-78], a mixture of carbon monoxide and hydrogen is obtained.

For this CO + H_2 mixture (after rearranging the molar ratio as needed) there are several uses of which we will refer only to some due to their high potential for future large-scale implementations:

- methanol synthesis [48];
- production of hydrogen [79, 80];
- production of aldehydes and alcohols through the OXO process [22, 23];
- synthesis gas for the Fischer-Tropsch process followed by developments of fuels, heavy chemicals and plastics [77, 81];

- production of electricity using molten carbonate fuel cells or solid oxide fuel cells: MCFC CONTEX and FC DISTRICT – NEW μ-CHP – two European projects in which the author participated as a specialist;
- production of dimethyl ether, a Diesel alternative fuel with a cetane number (CC 55) higher than that of diesel (CC 51);
- n-butanol synthesis [82-86] (obtained through the fermentation of flue gases – extracted from the discharge of large combustion plants and enriched with hydrogen and carbon monoxide), used then as an alternative fuel [87-89] or converted into heavy chemicals or plastics [90].

These being the data at present, there are only a few industrial processes that apply DRM (dry methane reforming) or CSDRM (combined steam dry methane reforming): CALCOR [91], SPARG (Haldor Topsøe) [92], Tri-reforming and Linde Gas. The main problem of the DRM process is the catalysts that must be resistant to coking.

This chapter presents the results of laboratory testing of some nickel catalysts in the DRM/CSDRM process.

II.2. Catalysts preparation

Three mesoporous nickel catalysts were prepared on a mesoporous alumina support by coprecipitation (CP), **Fig. 2.1.(a)** and sequential precipitation (SP), **Fig. 2.1.(b)** by a method described by a research group in south Korea [78]. The metal was dosed so that the percentage of nickel was 20%. Initially the catalytic activity of the catalysts was tested to produce hydrogen by steam reforming of liquefied natural gas. I decided to test their catalytic activity in the process of dry reforming CH_4 with CO_2. The catalysts were coded as 20Ni/Al_2O_3-CP, 20Ni/Al_2O_3-SP and 20Ni3Ce/Al_2O_3-SP, as shown in **Table 2.1.**

Table 2.1. – Description and coding of catalysts

Catalyst description	Metal load (%)	Preparation method	Code
Support	Ni – 0%, Ce – 0%	precipitation	S
20Ni/Al_2O_3-CP	Ni – 20%	coprecipitation	CP
20Ni/Al_2O_3-SP	Ni – 20%	sequential precipitation	SP
20Ni3Ce/Al_2O_3-SP	Ni – 20%, Ce – 3%		3CeSP

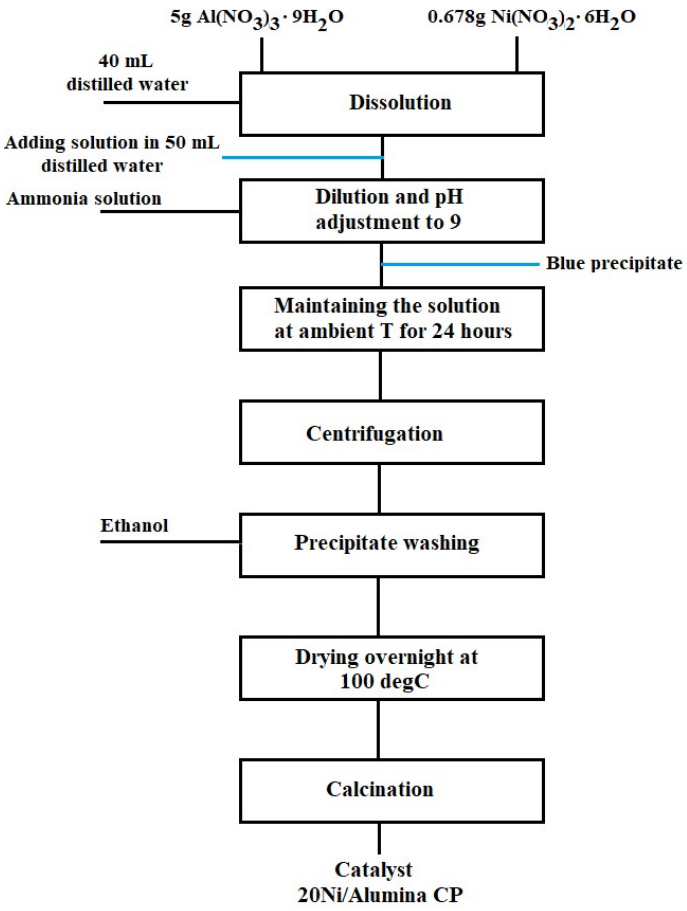

(a) Flow chart for the preparation of the 20Ni/Al_2O_3 – CP catalyst

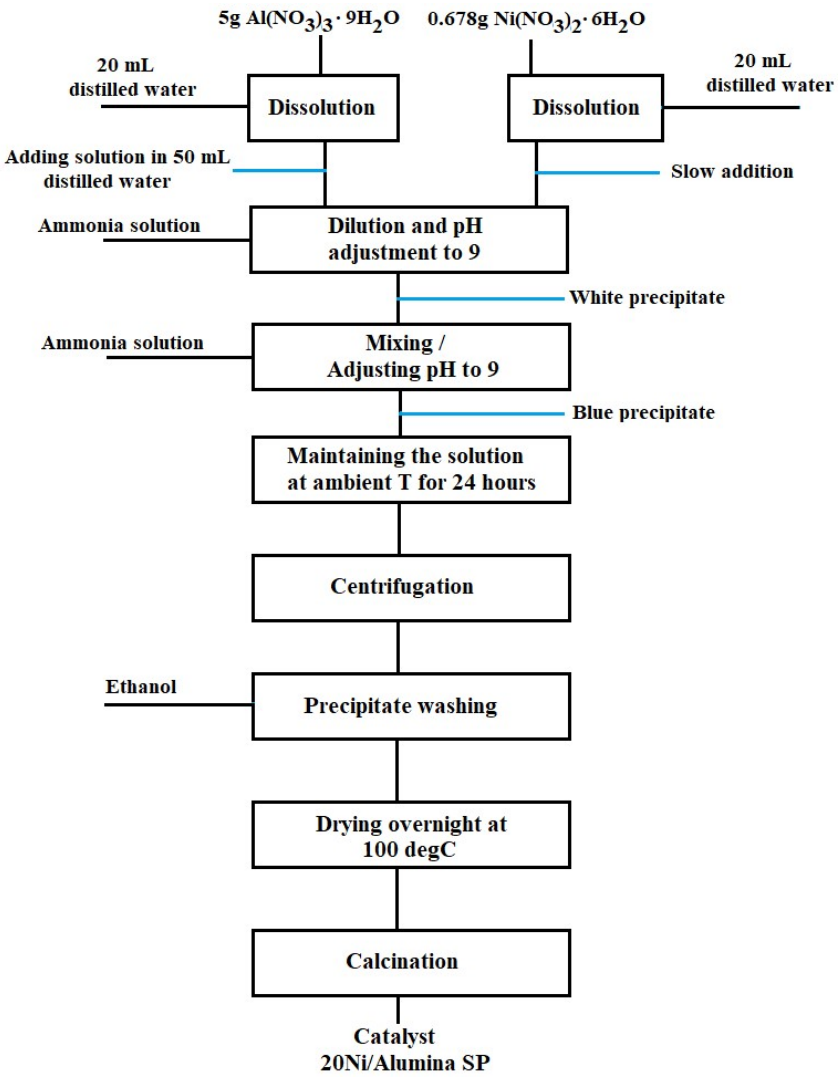

(b) Flow chart for the preparation of the 20Ni/Al_2O_3 – SP catalyst

Fig. 2.1. Preparation methods for catalysts 20Ni/Al_2O_3 – CP (coprecipitation) and SP (sequential precipitation)

The temperature program used for the calcination of catalysts comprises the following steps: (a) level 1 – 600 min, 100 °C, ramp 1 – 0.625 °C/min, to 250 °C; (b) level 2 – 60 min, 250 °C, ramp 2 – 0.833 °C/min, to 450 °C; (c) level 3 - 60 min, 450 °C, ramp 3 – 1.042 °C/min to 700 °C; (d) level 4 – 300 min, 700 °C.

CATALYST CHARACTERIZATION

The catalysts prepared within the activities related to this Chapter II (previously described in **Table 2.1.)** were characterized by the following physical-chemical methods: textural parameters, TGA, XRD, FTIR, TEM, EDX and catalytic activity testing and endurance tests.

II.3. Textural parameters of the catalysts

Liquid nitrogen was used to record N_2absorption-desorption isotherms for the three catalysts. **Fig. 2.2.** shows these isotherms and **Fig. 2.3.** shows the corresponding curves for the medium pores diameter, calculated by BJH from desorption side of the isotherms.

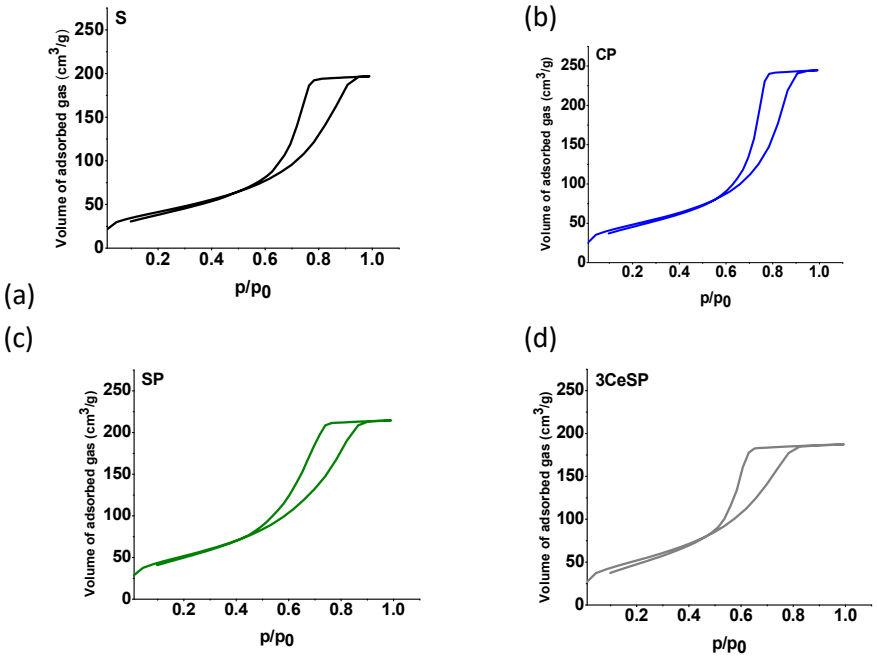

Fig. 2.2. N_2 adsorption-desorption isotherms with shapes of IV(a) H1 hysteresis type according to IUPAC (caused by capillary nitrogen condensation): (a) support – mesoporous alumina, (b) CP (coprecipitation), (c) SP (sequential precipitation), and (d) 3CeSP (sequential precipitation) [93, 94].

The final saturation plateau of the isotherms differs in the four charts above. The maximum level (on the vertical axis) is in the case of CP followed by SP: CP > SP > S > 3CeSP, data correlated with the pore volume and the length of the plateau (on the horizontal axis) which decreases in this order: 3CeSP > SP > S > CP (see **Table 2.2.** below).

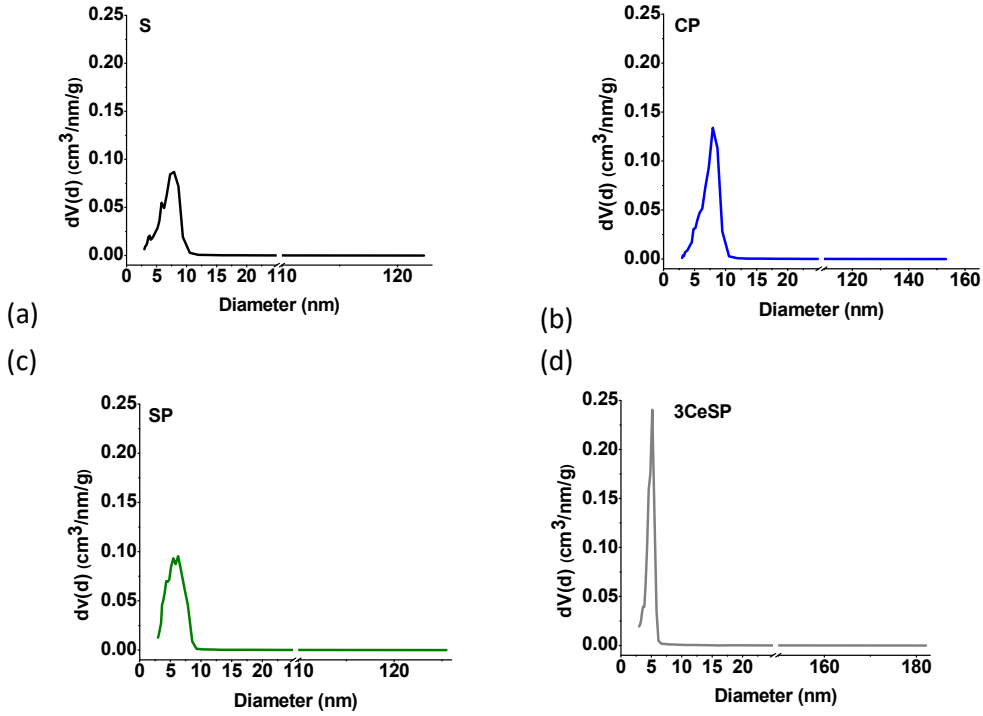

Fig. 2.3. Pore size distribution curves

To determine the specific surface area, S_{BET}, Brunauer-Emmett-Teller method was used, and average pore diameter, d_{BJH}, was computed by Barrett-Joyner-Halenda method from the desorption part of the isotherm. These parameters together with the total pore volume measured up to the relative pressure of 0.99 are given in **Table 2.2**.

Table 2.2. Textural parameters of support and catalysts

Catalyst	Surface area, S_{BET}, m^2/g	Pore volume, V_{tp}, cm^3/g	Average pore diameter, d_{BJH}, nm
S	191.449	0.321	7.902
CP	223.074	0.400	7.941
SP	256.670	0.355	6.258
3CeSP	264.557	0.317	5.146

S_{BET} decreases as follows: 3CeSP > SP > CP > S, but the pore volume decreases in a different order: CP > SP > S > 3SP. Also, d_{BJH} decreases from S to 3SP: CP > S > SP > 3SP. All these data suggest that some Ni crystallites are present in the pores of the support.

II.4. XRD

The fine ground catalysts were analyzed by the X-ray diffraction method. The data obtained by XRD analysis are represented in **Fig. 2.4.** (CP – bottom, SP – middle, and 3CeSP - top).

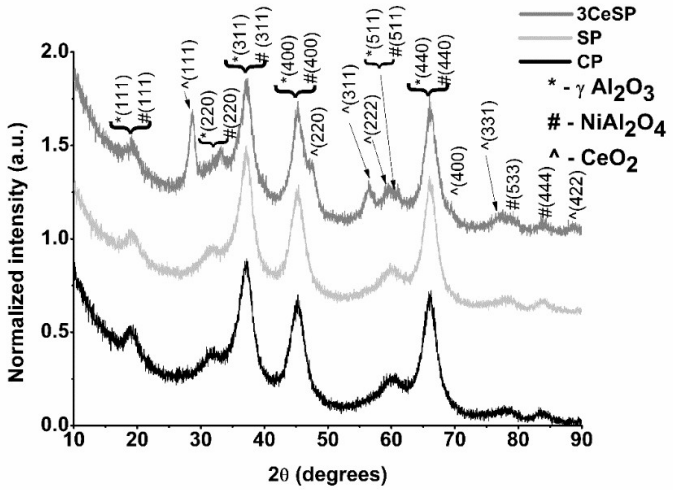

Fig. 2.4. XRD charts for the three catalysts studied

A first observation resulting from the interpretation of the three graphs in **Fig. 2.4.** is that the XRD diffractogram for CP and SP catalysts are almost identical even though the method of preparation differs.

As can be seen, compounds detected are as follows: (a) γ-Al_2O_3 (marked with *) JCPDS 00-010-0425 ([2θ°] - [hkl]: 19.4 – 111, 31.9 – 220, 37.2 - 311, 45.6 – 400, 66.9 - 440) [95]; (b) $NiAl_2O_4$ spinel (marked with #) JCPDS 78-1601 ([2θ°] - [hkl]: 19.6 – 111, 31.7 – 220, 37.5 – 311, 45.3 – 400, 60.2 – 511, 66.1 - 440) [96] and (c) CeO_2 (marked with ^) JCPDS 34-0394 ([2θ°] - [hkl]: 28.5 -111, 33.09 – 200, 47.5 – 220, 56.26 – 311, 58.9 - 222) [97].

$NiAl_2O_4$ spinel structure consists of metallic species of nickel dispersed on the support of γ-Al_2O_3 [96]. The detection of this spinel ($NiAl_2O_4$) in the XRD diffractograms above is proof of the strong interaction between metal and support, which implies a superior resistance to sintering and coking of the studied catalysts. Also, the fact that Al_2O_3 is in gamma form is appreciated. Thus, it tolerates on its surface large amounts of completely dehydrogenated carbides of carbon, reactive C_α species, resulting in higher CO_2 conversions [98, 99]. CeO_2 has an interesting role: it facilitates (at least theoretically) the access to the mobile oxygen species from the crystalline lattice of the catalyst, thus accelerating the oxidation reactions of the surface [100].

Crystallite size for all species present in the catalyst composition was calculated from XRD data. For these calculations, the Scherrer equation [34-36] was used and the calculations are presented in **Table 2.3**.

Table 2.3. Crystallite size determined from XRD data

Catalyst	Crystallite size, nm		
Species / 2θ°	γ-Al_2O_3, 37.2	$NiAl_2O_4$, 45.3	CeO_2, 56.3
CP	3.1	3.6	-
SP	2.9	3.0	-
3CeSP	3.1	3.6	3.6

As can be seen from **Table 2.3.**, the crystallite size values are approximately equal (within the range 2.9 – 3.6 nm), with a very small difference observed in the case of SP.

II.4. FTIR

From the FTIR spectra for Py adsorbed on the acid centers of the catalysts, represented in **Fig. 2.5.**, the segregation of the Lewis and Brönsted acid sites can be detected.

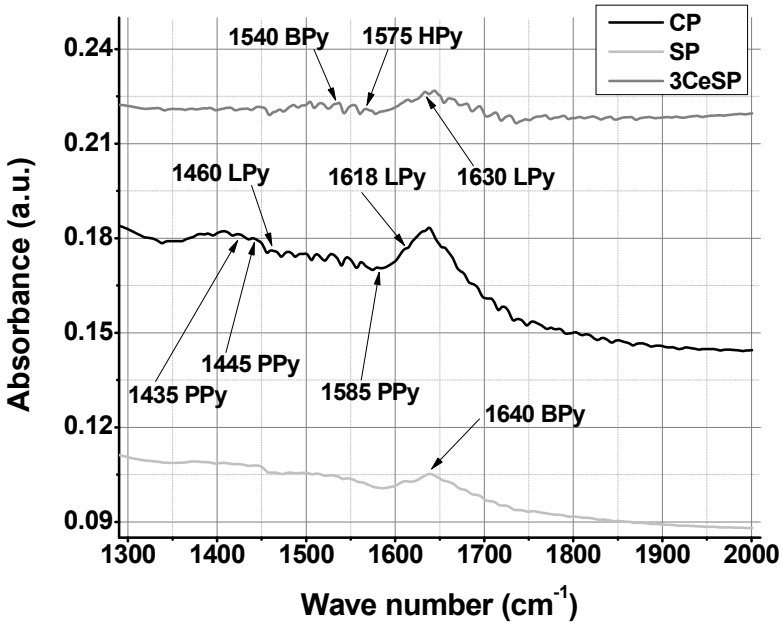

Fig. 2.5. FTIR spectra for Py adsorbed on Ni/Al_2O_3 catalysts: CP (middle), SP (bottom) and 3CeSP (top) in the 1300 – 2000 cm^{-1} range (P – physiosorbed, Py – pyridine, B – Brönsted, L - Lewis)

The band peaks characteristic of the Lewis and Brönsted acid sites appearing in the FTIR spectra of pyridine (Py) catalysts in **Fig. 2.5.** can be seen at the following wavelengths [30, 101]: (a) **1435** and **1445** cm^{-1} (twin bands) - v_{19b} - assigned to physiosorbed pyridine (PPy); (b) **1460** cm^{-1} - v_{19b} - characteristic for Py adsorbed on Lewis acid sites (LPy); (c) **1540** cm^{-1} - v_{19b} - peak area being proportional to the concentration of Brönsted acid sites (BPy); (d) **1575** cm^{-1} – v_{8b} - considered specific for acidic Brönsted HPy sites; (e) **1585** cm^{-1} – v_{8a} – Py molecules physiosorbed on catalyst acid sites (PPy); (f) **1618** and **1630** cm^{-1} – v_{8a} – characteristic for pyridine (Py) adsorbed on two types of Lewis acid sites (LPy); (g) **1640** cm^{-1} – v_{8a} – peak area is proportional to the concentration of Brönsted acid sites (BPy). These Brönsted acid sites may be of the type: -O-Al-O-H^+ , but they can also be protons generated by reducing Ni ions in hydrogen medium.

II.4. TEM

The TEM images for the three catalysts studied are represented in **Fig. 2.6.**

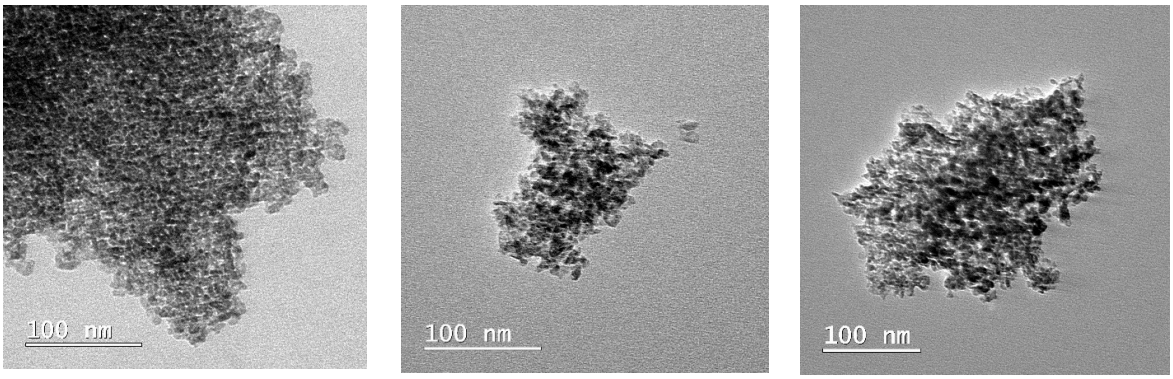

(a) **(b)** **(c)**

Fig. 2.6. TEM images for CP (a), SP (b), 3CeSP (c) catalysts

An analysis of the images in **Fig. 2.6.(a-c)** shows a good distribution of the active metal(s) on the support. The porosity is high for all three catalysts. However, the metal is distributed more evenly throughout the mass of the catalyst in the case of the CP catalyst, obtained by coprecipitation and represented in (a). The same cannot be said about the catalysts SP (b) and 3CeSP (c) obtained by sequential precipitation. In the case of these two catalysts, a large part of the metal(s) is distributed on the surface of the support.

II.5. Experimental setup and procedure

II.5.1. Conventional heating

The experimental setup (conventional heating) consists of two tubular furnaces placed in series with a quartz reactor on the interior as described in **Fig. 2.7**. The first furnace acts as a gas preheater (temperature fixed at 375 °C) and water vaporizer (when necessary) and the second one is the catalytic layer heater (variable temperature up to 900 °C). Gases are measured and adjusted using Sierra SMART TRAK50 gas controllers, mixed in a dynamic mixer (own design inspired by gas-gas burners) and then introduced into the quartz reactor in which the catalyst layer is located. The catalytic layer consists of a mixture of catalyst (0.5 g, ground to a particle size of 315 – 500 μm) and mineral wool (also 0.5 g, fine ground). The reaction products that leave the reactor are dehydrated and water is collected in a cooling trap (**Fig. 2.9.**). After dehydration, the reaction products go to a gas chromatograph for analysis (**Fig. 2.10.**).

The results of gas chromatography are calculated and expressed as conversions of the reactants and as yield of transformation of reactants into the useful product, CO.

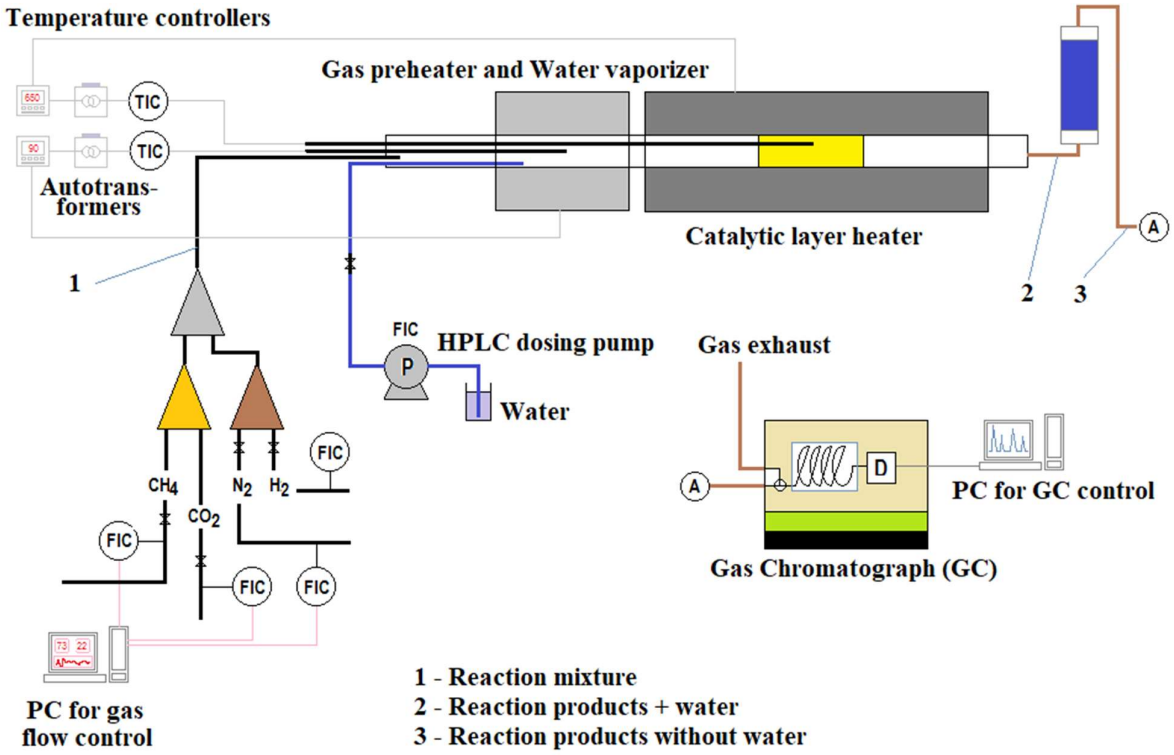

Fig. 2.7. Experimental setup – conventional heating

In **Fig. 2.8. – 2.10.** some details of the experimental setup are given.

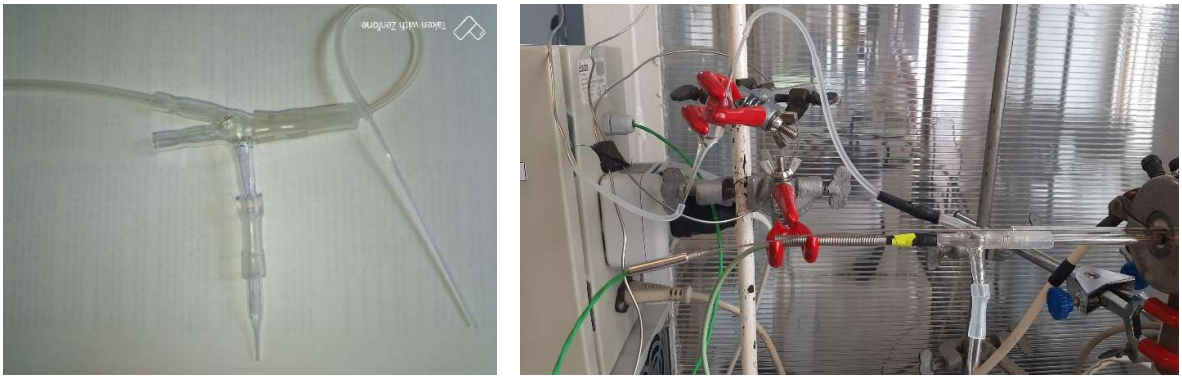

Fig. 2.8. The glass piece for introducing the reactant mixture and water into the reactor: on the left - T-Y piece with three inlets (top: water hose, middle: thermocouple, bottom: inlet for reactants mixture/hydrogen for regeneration) and one outlet. On the right - installation overview of the T-Y glass piece

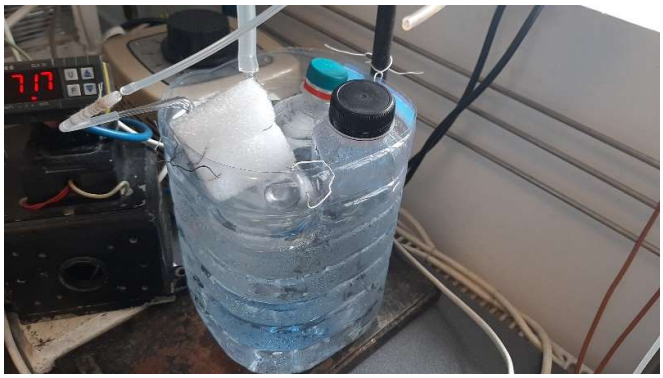

Fig. 2.9. Cooling trap (3 – 4 °C) to condense the water vapor leaving the reactor

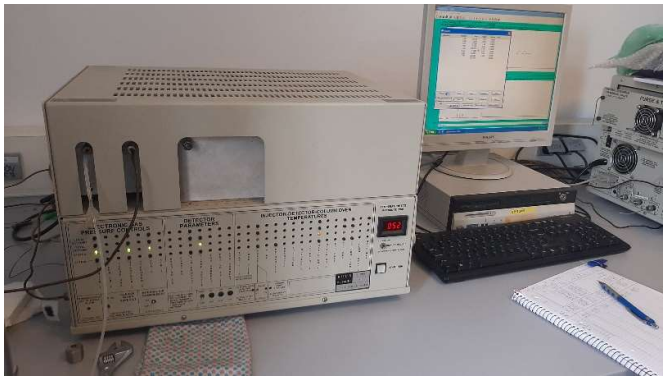

Fig. 2.10. Gas-chromatograph (left) together with the computer that controls it (right)

II.5.2. MW heating (microwave)

For heating of the catalyst in the MW field, the tubular furnaces described above have been replaced with the equipment described in the following **Fig. 2.11.**, the rest remaining unchanged:

(a)

(b)

(c)

(d)

(e)

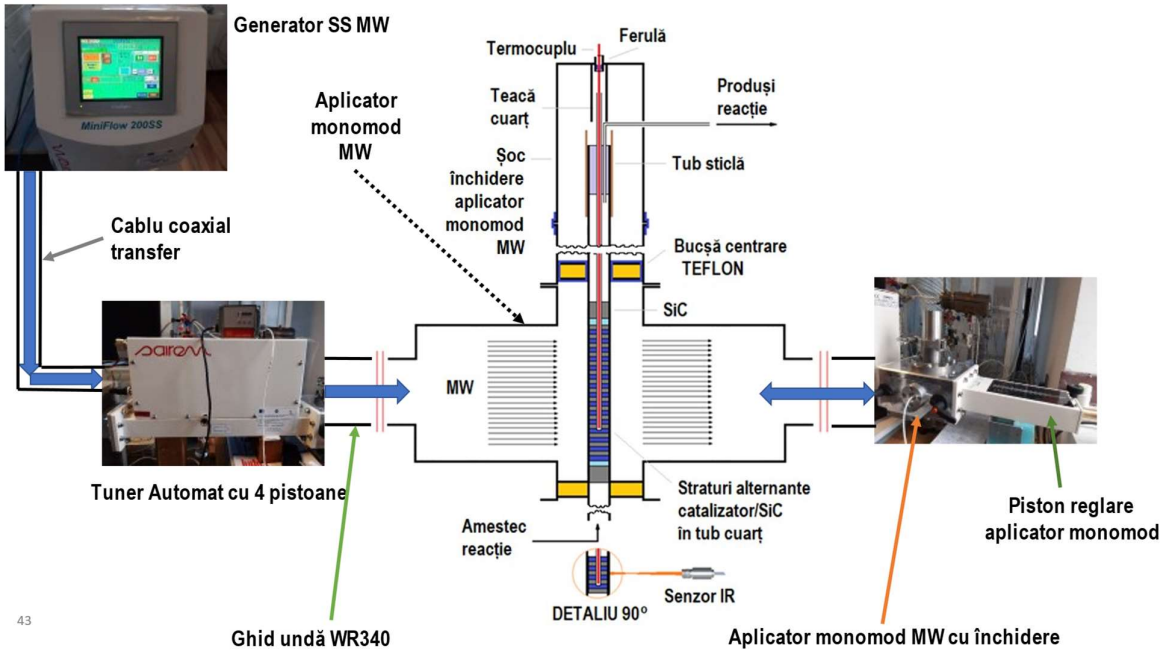

(f)

Fig. 2.11. (a) Polytechnic designed microwave generator (magnetron type) or (b) Solid-state microwave generator (Sairem, MiniFlow 200SS) connected (via WR340 waveguide) to (c) a 4-piston automatic tuner also connected (also via WR340 waveguide) to (d) a monomode cavity (unpainted metal) and piston system for wavelength adjustment and microwave applicator tuning.

The installation is a monomode microwave applicator, **Fig. 2.11.(f)**, where the microwaves are provided by a solid-state generator. The catalyst layer (consisting of a mixture as homogeneous as possible of catalyst: 1 g, finely ground and SiC: 4 g, coarsely ground, particle size 1-2 mm) is arranged in a quartz tube reactor with a diameter of 10 mm. The catalyst was uniformly mixed with SiC which provides the absorption of microwave energy. To measure the temperature, initially, an infrared sensor was used whose measurements were not always eloquent. When a metal thermocouple was inserted into the reactor, the applicator configuration had to be adapted to avoid the emission of microwave energy by the metal sheath of the thermocouple which can act as a (microwave antenna). A LibreVNA vector network analyzer was used to adapt the installation. This analyzer allows accurate measurement of reflected microwave power. To maintain optimal tuning during experiments, the installation also contains a 4-piston automatic tuner.

In **Fig. 2.11.(c)** and **(d)** it can be seen the Micro-Epsilon IR type temperature measurement system, CTM-3SF75H1-C3. Also, in **Fig. 2.11.(d)**, inserted into the microwave cavity can be seen the IR sensor, and in the back of the image appear the two tubular electric furnaces used in the conventionally heated installation. **Fig. 2.11.(e)** shows the exterior of the thermocouple measurement system and how it is connected to the equipment ground, while Fig. **2.11.(f)** is an overview of the installation.

II.6. Control parameters of the DRM process

The parameters calculated and monitored during the experimental work are defined by equation 2.1 and 2.2.

$$X_{CH4} = \frac{n_{i,CH4} - n_{f,CH4}}{n_{i,CH4}} \cdot 100 \qquad X_{CO2} = \frac{n_{i,CO2} - n_{f,CO2}}{n_{i,CO2}} \cdot 100 \qquad \text{Ecuatia 2.1}$$

$$\eta_{CO2 \to CO} = \frac{n_{CO}}{n_{i,CO2}} \qquad \eta_{T} = \frac{n_{CO}}{n_{i,CO2} + n_{i,CH4}} \qquad \text{Ecuatia 2.2}$$

in which:

X_{CH4} – conversion of methane,

X_{CO2} – conversion of carbon dioxide,

η_T – total yield of transformation of the reactants to carbon monoxide,

$n_{i, CH4}$ – initial number of moles of methane introduced into the reactor,

$n_{i, CO2}$ – initial number of moles of carbon dioxide introduced into the reactor,

n_{CO} – number of moles of carbon monoxide detected after the reactor.

II.7. ENDURANCE TESTS OF CATALYSTS – CONVENTIONAL AND MICROWAVE HEATING

The catalytic activity of the prepared catalysts: CP (coprecipitation), SP, and 3CeSP (sequential precipitation) was determined in the laboratory setup described in **Fig. 2.7**. The heat required for the DRM process was provided in two ways: conventional heating and MW heating. The conversion of carbon dioxide (X_{CO2}), conversion of methane (X_{CH4}), and the total yield of transformation of the reactants to carbon monoxide (η_T) were calculated and represented as a function of time in **Fig. 2.12** and **2.13** for each catalyst.

II.7.1. Conventional heating – endurance catalysts tests (1200 minutes)

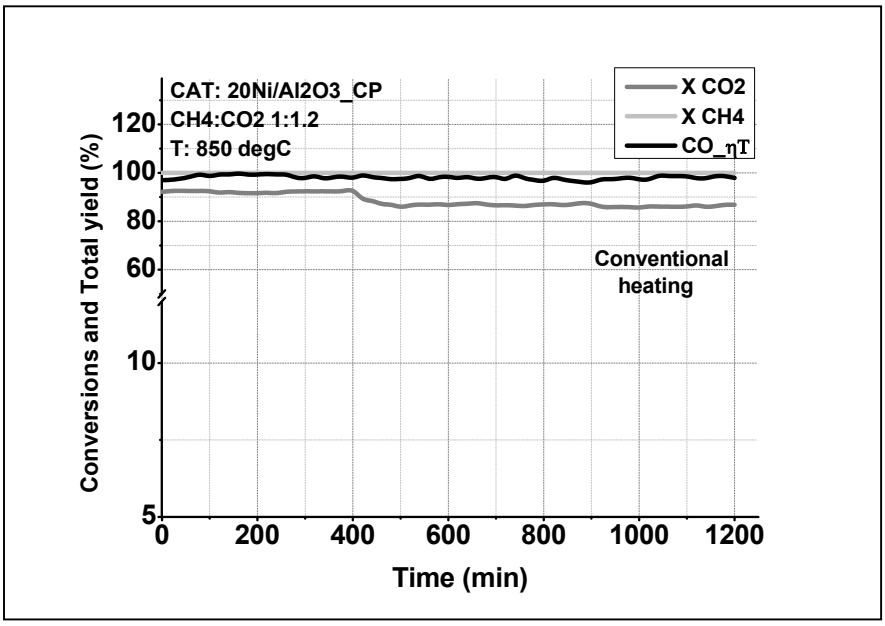

(a)

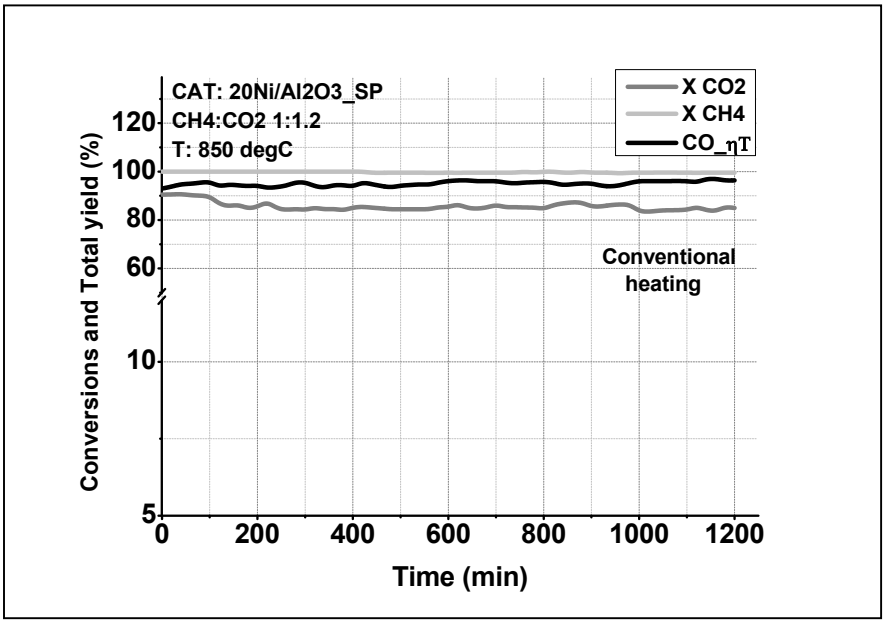

(b)

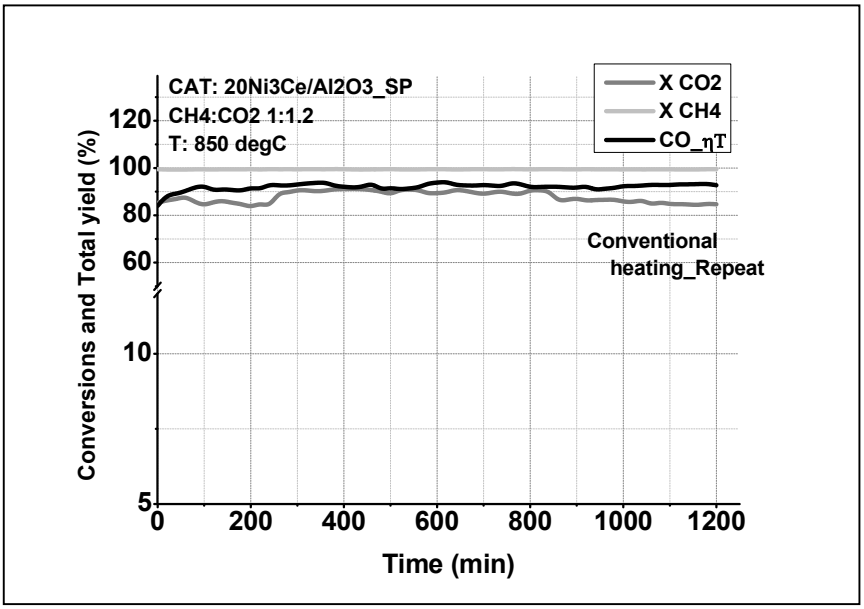

(c)

Fig. 2.12. Conversion of carbon dioxide, conversion of methane and total yield of transformation of the reactants to carbon monoxide for the three catalysts tested in conventional heating

As can be seen from the three diagrams in **Fig. 2.12.** the best performance belongs to the catalyst obtained by coprecipitation.

II.7.2. Microwave heating – endurance catalysts tests (1200 minutes)

In the three experiments described below, the temperature measurement was taken with an infrared sensor.

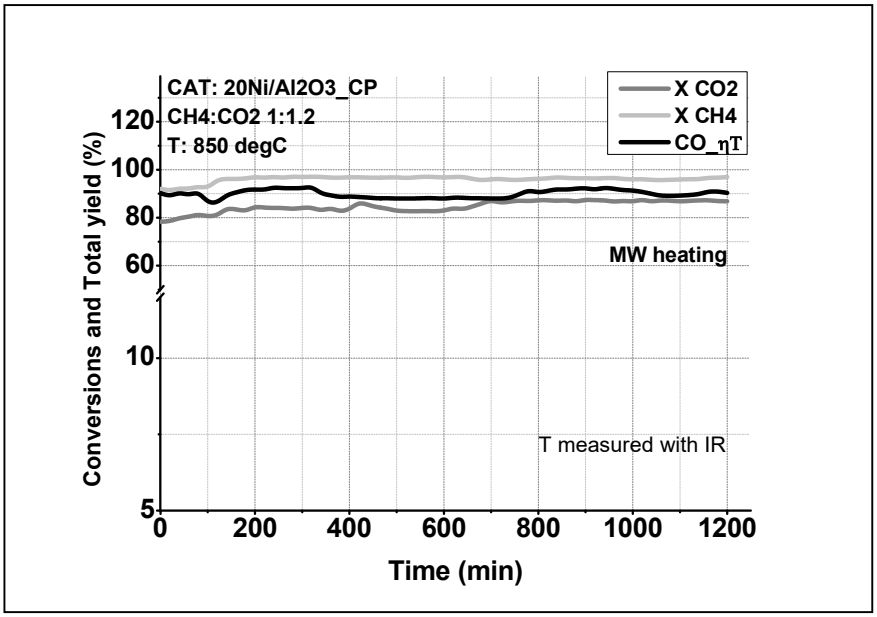

(a)

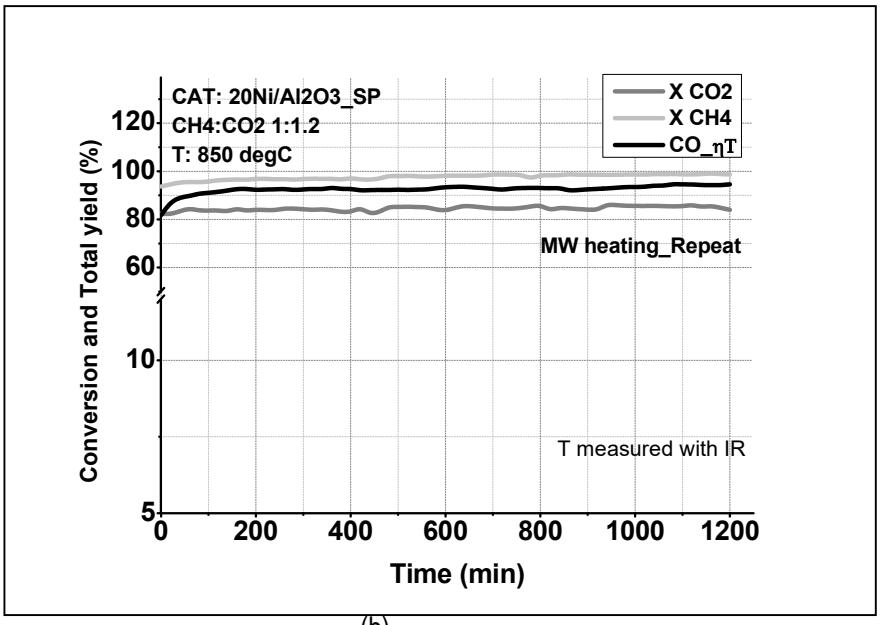

(b)

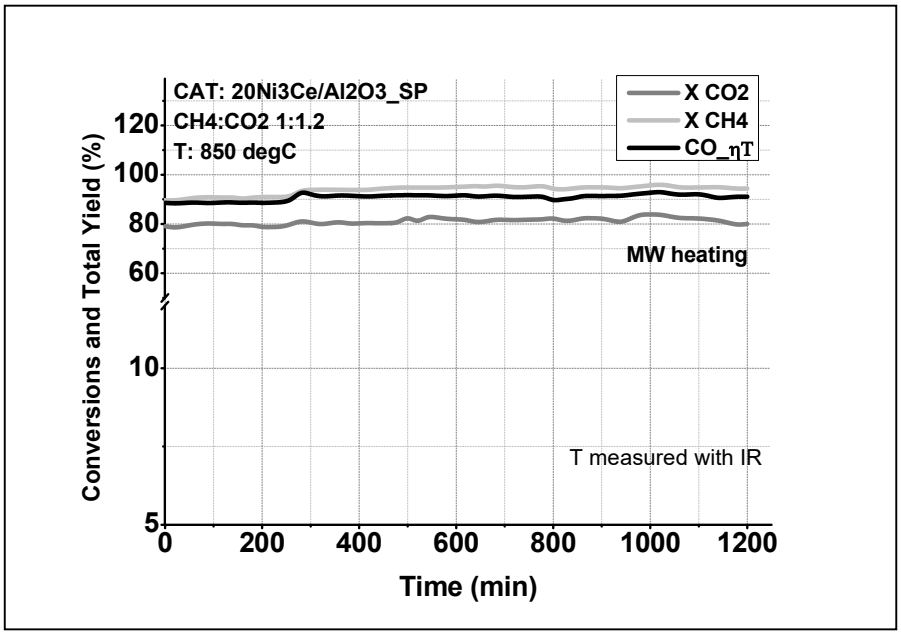

(c)

Fig. 2.13. – Conversion of carbon dioxide, conversion of methane and total yield of transformation of the reactants to carbon monoxide for the three catalysts tested in microwave heating

In the three diagrams in **Fig. 2.13.** the endurance tests for the three catalysts are presented, the heating being offered by a microwave field provided by a magnetron-type equipment represented in **Fig. 2.11.(a)**. An infrared sensor was used to measure the temperature. **The measurements of this sensor were not always eloquent.**

So, the decision was made to measure the temperature of the catalytic layer (with heating provided by microwaves) with a metal thermocouple. Several geometries of the monomode microwave applicator

were tried until the best geometry variant was obtained. The functional constructive variant is the one in **Fig. 2.14**.

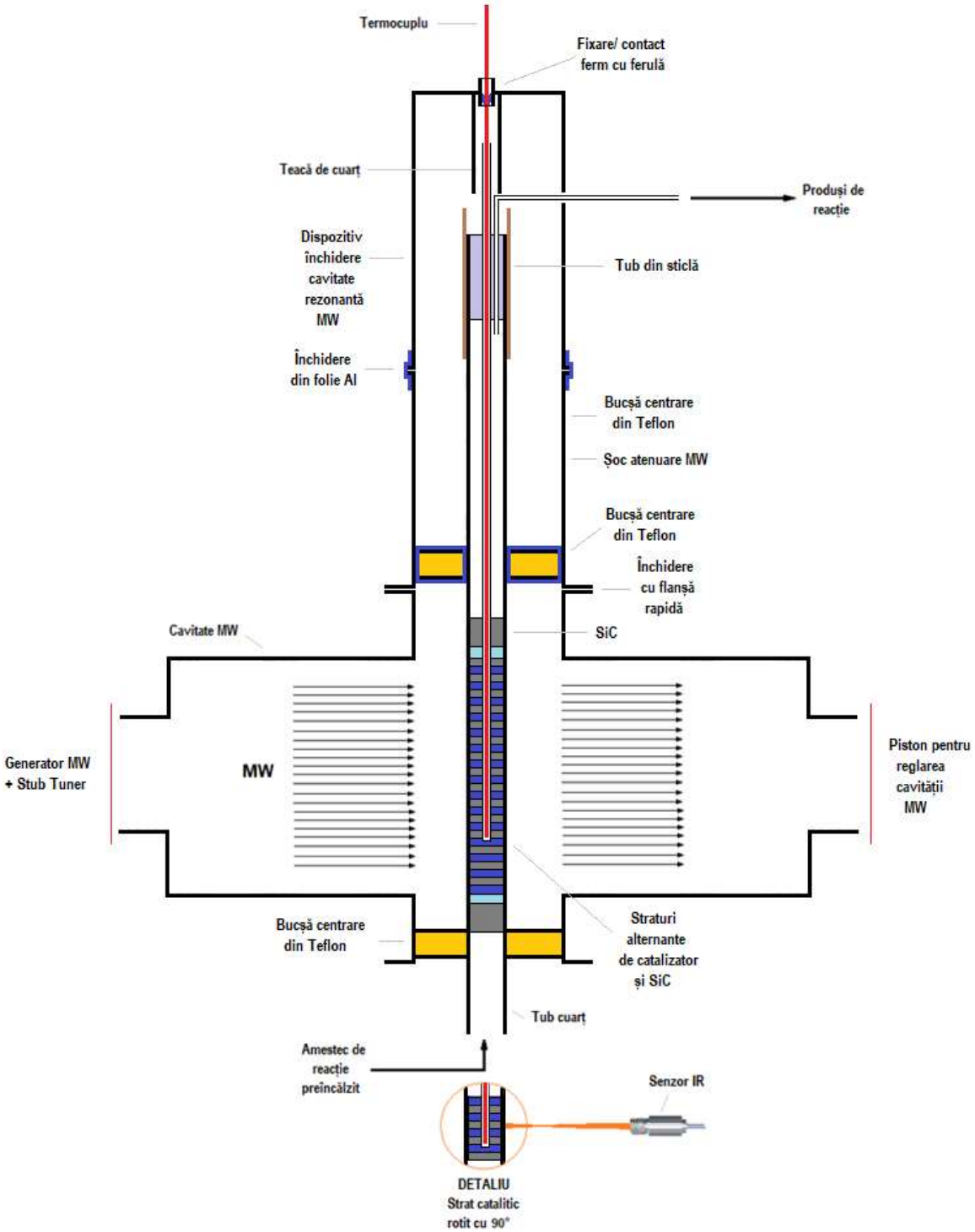

Fig. 2.14. Constructive variant with a centering nut covered in aluminum foil and a glass insulation tube in the upper part of the reactor

An endurance test of 20Ni/Al_2O_3-CP catalyst in the DRM process was performed in which for the first 2000 minutes the catalyst was heated in a microwave field (provided by a Sairem solid-state

microwave generator represented in **Fig. 2.11.(b)** and **(f)**) and in the following 2000 minutes the catalyst was heated conventionally with the help of electric furnaces represented in **Fig. 2.7., 2.8.** and **2.11.(d)**. It should be noted that between the two stages the catalyst was not regenerated and that the second stage started approximately 1 hour after the end of the first stage.

The results of the endurance test are represented in the combined diagram in **Fig. 2.15**.

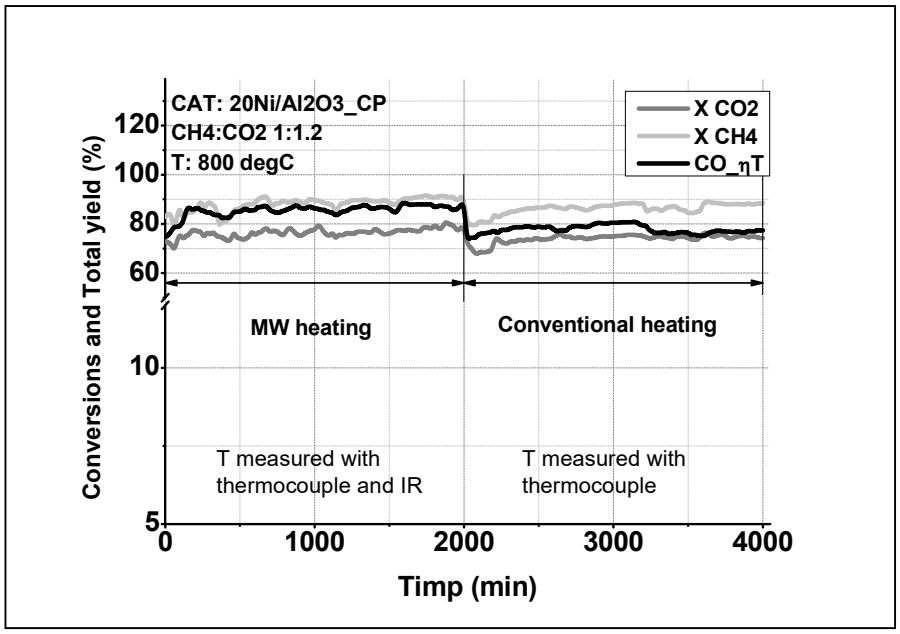

Fig. 2.15.– Endurance test for 20Ni/Al_2O_3-CP catalyst over 4000 minutes (just over 66 hours) at 800 °C

When analyzing the results from **Fig. 2.15.** it is observed that the values of the control parameters of the process of dry reforming of methane with carbon dioxide are noticeably higher when the catalyst was heated in the microwave field compared to the values obtained when the catalyst was conventionally heated. This could be explained with the help of the Hot SPOT theory [102].

If in the diagram in **Fig. 2.12.a**, at 850 °C, conventional heating, the catalyst loses part of its activity, in microwave heating, at 800 °C, **Fig. 2.15.**, this downward trend is no longer visible.

As a recapitulation of the results obtained during the endurance tests for the three prepared Ni-on-Alumina catalysts (20Ni/Al_2O_3-CP-coprecipitation, 20Ni/Al_2O_3-SP-sequential precipitation and 20Ni3Ce/Al_2O_3-SP- sequential precipitation), from the experimental data the following conclusions were reached:

- the catalyst obtained by coprecipitation: 20Ni/Al_2O_3-CP has the best catalytic activity and stability over time at conventional heating, temperature of 850 °C and molar ratio CH_4:CO_2 1:1.2.
- the catalytic activity for the 20Ni/Al_2O_3-CP catalyst is higher when heated in the microwave field compared to conventional heating, which can be explained by the Hot-SPOT theory.

Chapter III.

Ultrasonic or Microwave Cascade Treatment of Liquorice Root Waste - *Glycyrrhiza radix* – to intensify the process through severe ultrasound and microwave treatments

OBIECTIVE

O6. Valorization of technological waste of Liquorice (root) – *Glycyrrhiza glabra* – with the help of ultrasound and microwave assisted extraction;

O7. Enzymatic hydrolysis of lignocellulosic waste treated with ultrasound and microwaves in a 0.5 N NaOH solution.

III.1. Introduction

Lignocellulosic biomass is the most abundant renewable resource worldwide. The structure of lignocellulose is comprised of cellulose, hemicellulose, and lignin, which are all valuable biomaterial resources [103, 104].

Biomass refers to the biodegradable part of products, waste, and residues from agriculture, forestry, and related industries, as well as industrial and municipal solid wastes. Lignocellulosic biomass is comprised of any renewable organic material from terrestrial plants (energy crops (conventional food crops and non-food energy crops) and forest products) and aquatic plants (algae and seagrass), as well as organic waste and residues from agriculture, pisciculture, silviculture, municipal solid waste, and other wastes [105]. The industrial extraction of natural principles from medicinal plants results in a lignocellulosic residue which is not suitable for animal feed. Thus, this material is considered to be waste and an environmental threat. Currently, there is no proper waste management of such plants (e.g., licorice); they are burned, buried, or used to obtain biogas [51, 52, 106]. Thermochemical processing (e.g., pyrolysis and gasification) is an alternative for the conversion of such lignocellulosic biomass waste into fuels, building blocks, etc.[107-117].

With increasing energy prices (and amid the 2022 natural gas crisis) and the drive to reduce CO_2 emissions [44, 50], it is necessary, for economic sustainability, to find new technologies and new process strategies which reduce energy use and maximize valorization of raw materials. The conventional methods used to extract valuable compounds from vegetal materials require relatively high solvent and energy consumptions, long extraction times, or high temperatures that could lead to the targeted compounds degradation. Moreover, regarding the negative impact of organic solvents on the environment, it is necessary to use green solvents, such as water, for the recovery of valuable compounds [118]. In recent years, amongst others, efficient extraction processes, such as ultrasound- [119, 120] and microwave-assisted extractions [16, 121-123] have been developed.

The cavitation phenomenon can promote disruption of cellular tissue leading to an increase in mass transfer rate [16], as shown in **Fig. 3.1.a**. Considering vegetal material and extraction solvent, during microwave treatment, vegetal material can be heated selectively. Thus, the osmotic pressure that is created inside a vegetal particle ruptures the cell wall, and therefore results in easy release of the bioactive compounds [9, 121, 124, 125], as represented in **Fig. 3.1.b**.

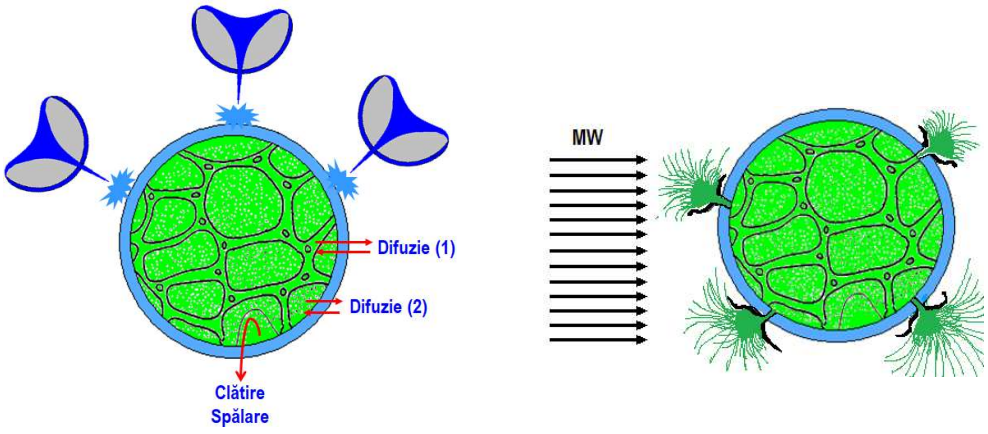

(a) (b)

Fig. 3.1. – Graphical illustration of the phenomena occurring during ultrasound-assisted [16] (a) and microwave-assisted (b)

In addition to bioactive compounds, described in Thesis (Chapter V) [126-130] *Glycyrrhizae radix* waste contains lignocellulose, which is a resourceful biomaterial part that can be converted to pentoses and hexoses or other valuable compounds after removing the lignin. An ultrasound- or microwave-assisted alkali pretreatment of lignocellulosic biomass to remove lignin can enhance the yield of monosaccharides obtained after the enzymatic hydrolysis of vegetal material [125].

In this study, we present a strategy for the valorization of lignocellulosic waste that results from the industrial extraction of active principles in water [126]. The first step of this strategy is the extraction of the residual bioactive compounds from the waste, using ultrasound and microwave treatments. The second step to valorizing these wastes is the pretreatment with ultrasound and microwave to render the waste suitable for the enzymatic hydrolysis of cellulose and hemicellulose to hexoses and pentoses.

III.2. US Treatment Equipment and Procedure

The severe US treatment of raw materials was performed using a dual-frequency reactor (**Fig. 3.2.**) equipped with a batch reactor of 600 mL and a stirring system. The US frequencies were 16 and 20 kHz and the maximum power of the two generators was approximatively 600 W.

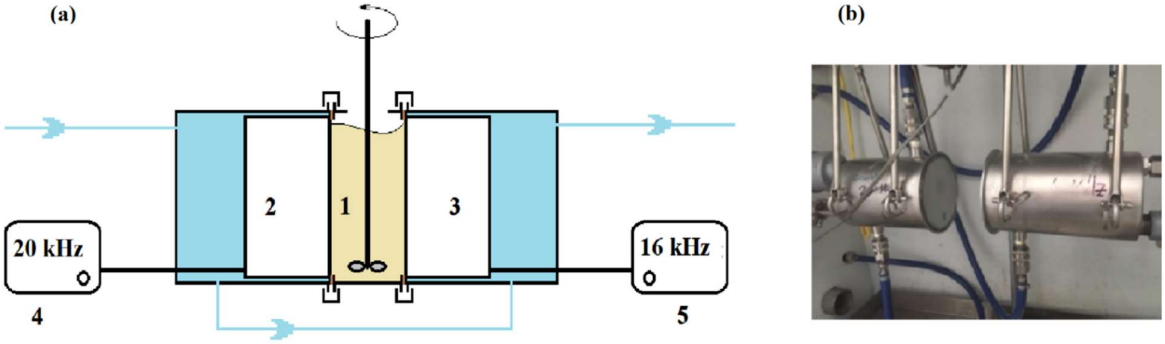

Fig. 3.2. – The schema (a) and picture (b) of the dual-frequency reactor equipment (DFR) for the severe US treatment (1 – batch reactor fixed with sanitary flange by the two ultrasound transducers, equipped with stirring system; 2, 3 – ultrasound transducers of different frequencies, cooled with water; 4,5 – ultrasound power control systems)

For *Glycyrrhizae radix*, the ultrasound treatment was performed for a 10:1(V: m) ratio of solvent to plant material. The extraction was carried out at a temperature of 25 °C for 5 and 15 minutes, using an

ultrasound power of 600 W for each transducer. Since both transducers are cooled with water during operation, the temperature increase is of maximum 2 - 5 °C.

III.3. Microwave Treatment Equipment and Procedure

The severe MW treatment of raw materials was performed using the Synthwave equipment (**Fig. 3.3.**). This apparatus may also be used to generate extreme values: temperatures and pressures up to 300 °C and 200 atm, respectively. Pressurization with an inert gas at such high pressures ensures maintaining the liquid phase of the sample. The equipment may also work with a reactor with a volume of maximum 900 mL.

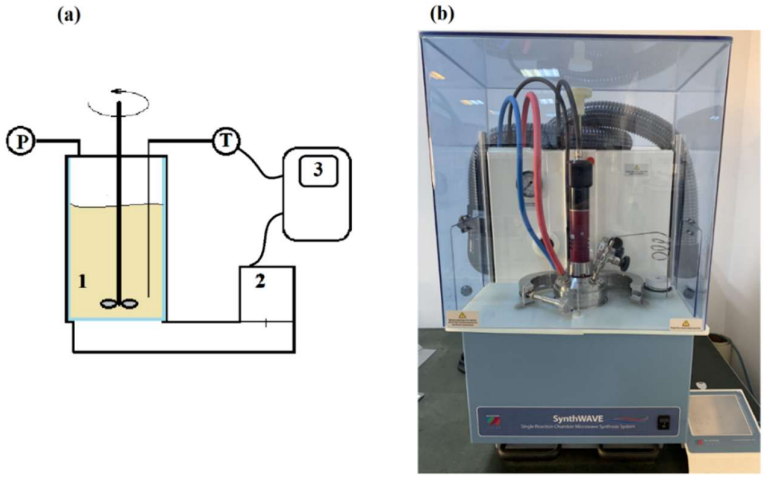

Fig. 3.3. - Schema (a) and picture (b) of the Synthwave equipment for the severe microwave treatment (1 - pressurized reactor equipped with stirring system, temperature, and pressure control systems; 2— microwave generator which transmits the microwaves to the reactor through a waveguide; 3 – control system which adjusts the microwave power in accordance with the temperature in the reactor)

The microwave treatment was performed at different temperatures (110, 120, and 150 °C) and a pressure of 6 – 10 atm (higher than vapor pressure of water at reaction temperature). The inert gas used was argon. The experiments were carried out for a 10: 1 (V: w) ratio of solvent (water or 0.5 N NaOH solution) to plant material. The extraction time was 30 and 60 min and started after the mixture reached the working temperature. The microwave power required that a constant temperature be maintained in the ranges of 150 – 200, 200 – 300, and 375 – 425 W for 110, 120, and 150 °C, respectively. The frequency was 2.45 GHz, for all the microwave treatments.

After the US and MW treatments, the samples were left to settle for one hour before vacuum filtering. The filtrate was subjected to soluble lignin or active principles content determination. Prior to the enzymatic hydrolysis, the solid material was washed with distilled water up to a neutral pH and dried at 50 °C for 8 – 16 h using a heating oven. The strategy for the US and MW treatments is shown, as a logic diagram, in **Fig. 3.4.**

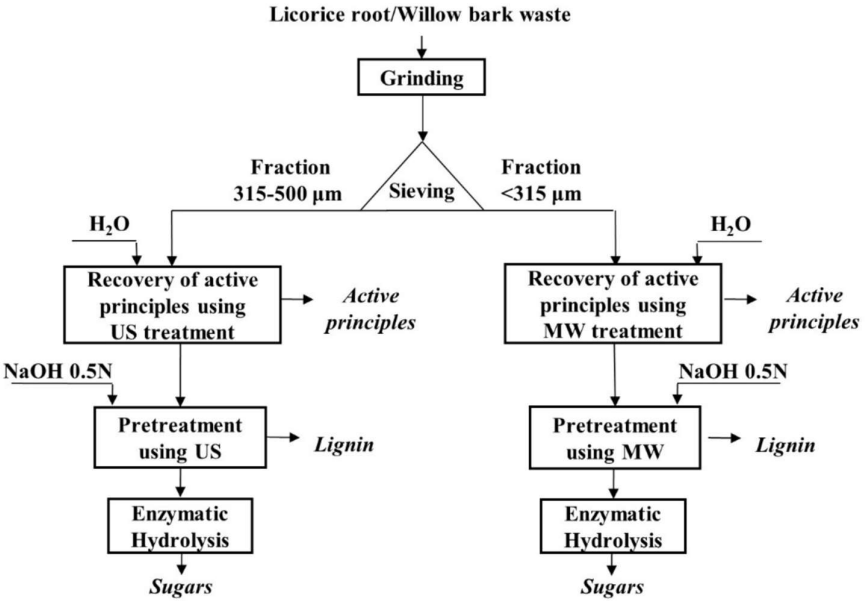

Fig. 3.4. – Logic diagram of the industrial lignocellulosic waste valorization using the ultrasound and microwave treatments.

III.4. Waste delignification

Lignin from the lignocellulosic waste materials was extracted to enrich the waste in cellulose in order to prepare it for the enzymatic hydrolysis to sugars. The ultrasound and microwave treatments were performed using a solution of 0.5 N NaOH in water.

III.5. Enzymatic hydrolysis procedure

Enzymatic hydrolysis requires a pH value of 5. Therefore, the treated lignocellulosic material for delignification is mixed with a buffer solution containing citric acid and sodium phosphate dihydrate to maintain a constant pH. The experiments are carried out in Erlenmeyer vessels with a 25:1 (V: w) ratio of buffer solution to plant material. Celluclast 1.5 L enzyme (0.7 mL per gram of substrate) is added into each vessel (the enzyme dosage was chosen based on preliminary tests from ULTRAMINT project). The mixtures are stirred at 120 rpm for 48 h using a reciprocating shaker at a temperature of 50 °C. During the reaction, samples are taken at 24, 48, and 72 h intervals, in separate vials, and quickly immersed in boiling water to deactivate the enzyme. The reaction mixtures are centrifuged at 3500 rpm for 10 min, and the supernatants are further analyzed to determine the saccharide concentrations.

RESULTS AND DISCUSSION

III.6. US and MW Extractions of Active Principles from the Lignocellulosic Materials

The first step taken in this chapter was to verify the efficiency of ultrasound and microwave extractions of the active principles from the technological waste: glycyrrhizic acid from the root of *Glycyrrhiza glabra*. The results are presented in **Fig. 3.5.**

According to the Romanian Pharmacopeia, the total content of glycyrrhizic acid in licorice root is 33.82 mg/g DM. Experiments performed using ultrasound and microwave for the extraction from waste materials showed that up to 6.5 mg/g DM of glycyrrhizic acid could be extracted, meaning that the targeted

compound was still present in the industrial waste and could be valorized. The higher content of glycyrrhizic acid from licorice root waste was achieved by applying the microwave treatment for 30 min at a temperature of 120 °C (**Fig. 3.5.b.**); however, a similar value was obtained for the ultrasound treatment at only 25 °C for 15 min (**Fig. 3.5.a.**).

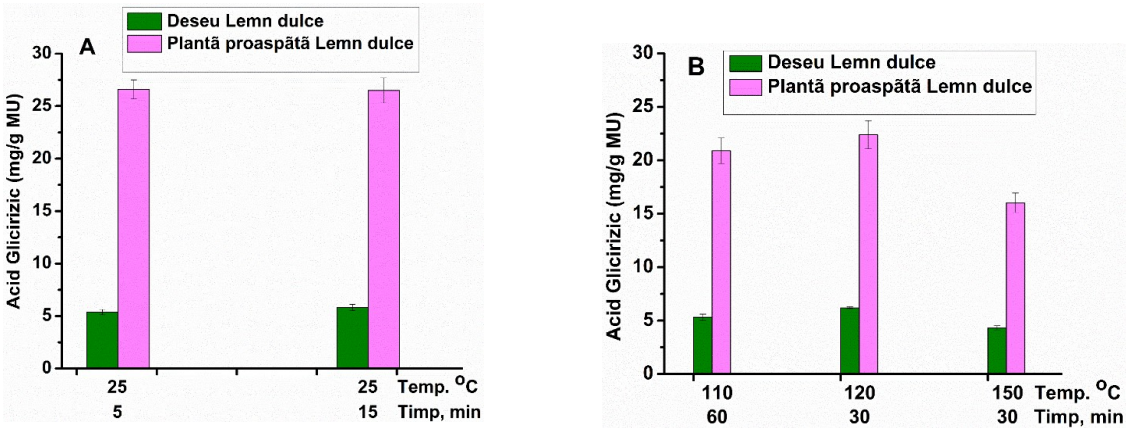

Fig. 3.5. – Content of active principles from *Glycyrrhiza radix* lignocellulosic waste extracts (a) ultrasound and (b) microwave

III.7. Delignification and Enzymatic Hydrolysis of Glycyrrhizae radix

Another strategy for the valorization of lignocellulosic waste (which has already been processed to extract the active principles) is delignification followed by enzymatic hydrolysis of cellulose to further obtain sugars. The ultrasound and microwave pretreatment efficiency is monitored by the amount of lignin removed and, secondly, by the determination of the concentrations of saccharides that result after enzymatic hydrolysis. The delignification efficiency is shown in **Fig. 3.6.**

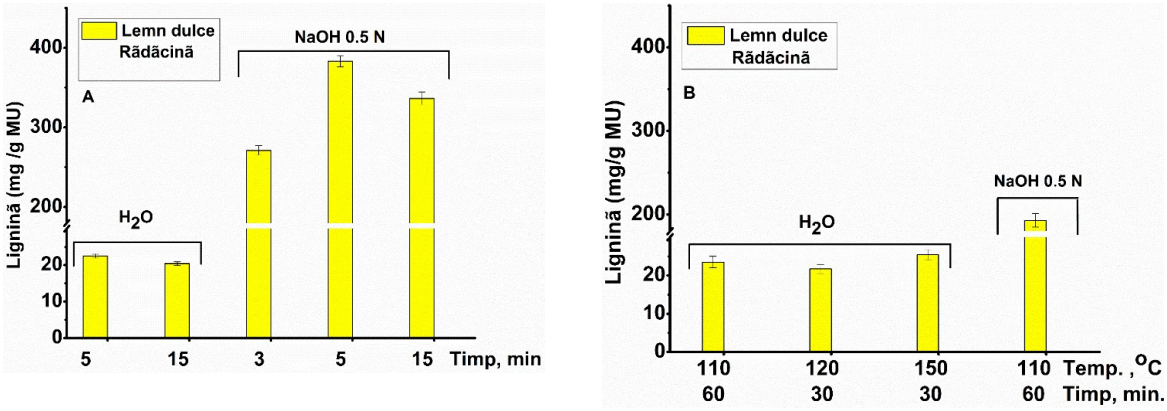

Fig. 3.6. - Soluble lignin concentration of the vegetal waste extracts: (a) treated with ultrasound; (b) treated with microwave

An analysis of the data from **Fig. 3.6.** shows that the best solvent for delignification is the 0.5 N NaOH solution, for both ultrasound (**Fig. 3.6.a**) and microwave (**Fig. 3.6.b**) treatments. The soluble lignin concentration after US treatment in the NaOH solution was approximatively seventeen times higher than the one performed in water. Considering the US treatment time, the best results were achieved for 5 min (**Fig. 3.6.a**). The microwave treatment in NaOH solution leads to a concentration of soluble lignin that is approximatively eight times higher than the one carried out in water (**Fig. 3.6.b**).

The results of the enzymatic hydrolysis of delignified lignocellulosic waste are shown in **Fig. 3.7.** Although the delignification of *Glycyrrhizae radix* waste by the microwave treatment is lower as compared with that by the ultrasound treatment (**Fig. 3.6.**), it leads to satisfying results for the enzymatic hydrolysis (a saccharide concentration of only 5% lower is achieved for an enzymatic hydrolysis time of 72 h).

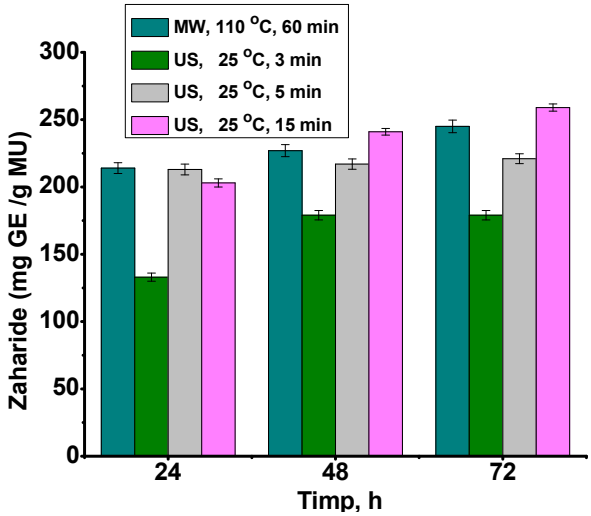

Fig. 3.7. - Saccharide concentrations after the enzymatic hydrolysis of lignocellulosic *Glycyrrhizae radix* waste treated with ultrasound and microwave in a 0.5 N NaOH solution

Energy Consideration

Table 3.1. shows the energy consumption of each type of equipment used to treat the medicinal plant waste. It can be observed that they are comparable. If the use of such installations is considered on a pilot or industrial scale, then, batch reactors can be used for the microwave treatment and due to the shorter residence time, continuous reactors can be used for the US treatment. For such installations, the energy consumption can be significantly lower than the one obtained on a laboratory scale.

Table 1. Energy consumption for each equipment used for the medicinal plant waste valorization

Equipment	Grid power (kW)*	Time (min)	Energy consumption (kWh)
US	1.2	5	0.1
		15	0.3
MW	0.35	30	0.175
		60	0.35

* Measured by a wattmeter

CONCLUSIONS

- Ultrasound applied in the preparation stage of Cu/SiO_2 catalysts led to:
  - a greater uniformity of copper deposition on the surface of the support in the case of the US10 catalyst compared to the conventionally prepared catalyst;
  - a higher selectivity to the useful product (butyraldehyde, 98.2%, in the case of the US10 catalyst compared to the conventionally prepared catalyst, 91.6%;
  - a lower selectivity to secondary products (butene, 1.7%, and dibutyl-ether) in the case of the US10 catalyst compared to the conventionally prepared catalyst (selectivity to butene, 8.3%).
- A Cu/Al_2O_3 catalyst (prepared from copper nitrate precursor) was obtained with a very high selectivity to butene, 95%, at a n-butanol conversion of 91.2%.
- The catalytic activity results for the $20Ni/Al_2O_3$ type catalysts are very encouraging. Endurance tests of alumina-supported nickel catalysts performed in microwave heating (800 °C) produce better process control parameters than conventional heating (850 °C).
- Endurance tests during 4000 minutes (2000 minutes heating in microwave environment and 2000 minutes conventional heating) justify the obtaining of a high-performance catalyst, $20Ni/Al_2O_3$ – CP (obtained by coprecipitation), for the dry reforming of CH_4 with CO_2. If the catalyst heated conventionally at 850 °C loses some of its activity, in microwave heating at 800 °C, this downward trend is no longer visible.
- Liquorice (root) waste still contains recoverable active principles through ultrasound and microwave treatments after the initial conventional extraction:
  - 6.2 mg/gMU glycyrrhizic acid (18% of the original content of 33.82 mg/gMU).
- The ultrasound or microwave pretreatment was very effective for the removal of lignin, which made it possible to convert the lignocellulosic biomass (considered waste by HOFIGAL SA up to now) to saccharides thus obtaining:
  - 250 mg/gMU saccharides from Liquorice (root) waste.
- Energy consumption is similar for both treatments:
  - US – 0.1 kWh/5 min and 0.3 kWh/15 min;
  - MW – 0.175 kWh/30 min and 0.35 kWh/60 min.

PERSPECTIVES

- **To continue research regarding the dry reforming of CH_4 with CO_2 for other catalysts**

Dry reforming of CH_4 with CO_2 is a complex process in which the catalyst plays a decisive role. So far, I have tested five catalysts with conventional heating (tube electric furnace): 10Ni/ZSM-5, 10Ni/SBA-15, 20Ni/Al_2O_3-CP, 20Ni/Al_2O_3-SP and 20Ni3Ce/Al_2O_3-SP. With heating provided by the energy of a microwave field, I have tested only one catalyst: 20Ni/Al_2O_3-CP.

That is why, I consider it opportune to continue the experiments by testing other catalysts through combined endurance tests: microwave heating, followed by conventional heating for the catalysts prepared by sequential precipitation 20Ni/Al_2O_3-SP, 20Ni3Ce/Al_2O_3-SP respectively the use of other promoters in addition to Cerium, such as: Lanthanum, Yttrium or Ruthenium.

- **To identify the opportunities to scale up the catalytic reactor for microwave assisted dry reforming of CH_4 with CO_2**

For a technology to be applied at an industrial level, it is necessary for it to reach different levels of maturity during the R&D and implementation phase. I believe that at the laboratory level I could take the research to a higher scale than the one I have already worked on: work with quartz reactors of larger diameters, with larger amounts of catalyst and implicitly with higher flow rates of reactants. I also consider a challenge to overcome the difficulties related to the heating of a larger amount of catalyst in the microwave field: to identify possibilities for improved control of the microwave power provided by higher power microwave generators: magnetron or solid-state and to adapt the configuration of monomode microwave applicators.

I wish I could also go through and complete TRL4 stage (Technology validated at laboratory scale).

- **Publication of the experimental data obtained during the study of the dry reforming of CH_4 with CO_2**

The article is in an advanced stage of drafting (90%):
Chisega-Negrilă C-G, Banu I, Trifan A, Vasilievici G, Trică B, Fierăscu R, Vînătoru M, Călinescu I, Catalytic activity of some nickel catalysts tested for production of synthesis gas by methane reforming with carbon dioxide. Conventional and microwave heating.

ORIGINAL CONTRIBUTIONS

I. Conversion of n-bio-butanol to butyraldehyde

- Developing a method for obtaining Cu/SiO_2 type catalysts in which the impregnation of the support with copper takes place in the presence of ultrasound.

- Synthesis in the presence of ultrasound (and testing in gas-phase dehydrogenation reaction of n-bio-butanol to obtain butyraldehyde) of a catalyst that had higher butyraldehyde selectivity (98.2% at 350 °C) than the one of a similar catalyst, but prepared conventionally (91.6% at 350 °C).

- Finding the experimental parameters to obtain; (a) a very uniform deposition of copper on the surface of the support, SiO_2, (b) dimensions in a very narrow range for the size of the deposited copper particles and (c) a lower acidity, in the case of the catalyst prepared in the presence of ultrasound.

- Setting up a classical determination method (by titration) of the overall copper content of the obtained catalysts.

- Finding the optimal experimental parameters for the dehydrogenation reaction of n-bio-butanol to bio-butyraldehyde: (a) flow rates of n-butanol and hydrogen, (b) temperatures for the n-bio-butanol vaporizer and reactor.

- Conception and realization of a glass cooling system (cooling agent: ethylene glycol) for the entire condensation train of the reaction products in order to be able to measure the total volume and mass of the condensable fraction of the reaction products: butyraldehyde, n-butanol, dibutyl ether and butene.

- Developing a method for gas chromatographic analysis of reaction products: (a) liquids – GC-FID and (b) non-condensable – GC-FID+TCD (FID – flame ionization detector and TCD – thermal conductivity detector).

- A method for segregating acid sites on the surface of the support, SiO_2, in Lewis and Brönsted acid sites and then segregating them into weakly acidic and strongly acidic Brönsted sites. The method uses thermogravimetric desorption of pyridine adsorbed on the acid sites of the support. Then, the infrared spectra with Fourier transform are recorded and interpreted for pyridine also fixed on these acid sites.

- Designing and making from glass of a gas-liquid mixer for the in-flow mixing of hydrogen and n-butanol.

- Explaining using analyzes such as: (a) X-ray diffraction (XRD), (b) energy dispersive spectroscopy (EDX), (c) nitrogen adsorption-desorption isotherms, (d) thermogravimetric analyzes (simple and with derivatization) (TGA-DTG), (e) thermal desorption of pyridine from the acid sites, (f) Fourier infrared spectra for pyridine fixed on the acid sites of the catalysts (FTIR), (g) scanning electron microscopy (SEM) of conversion of n-butanol and selectivity to dibutyl ether, butene, butyraldehyde and catalytic activity for the catalysts characterized in detail.

- Although not the subject of this thesis (but very promising for future n-bio-butanol chemistry), obtaining a Cu/Al_2O_3 catalyst (prepared from copper nitrate precursor) with a very high selectivity to butene (95%) at a high conversion of n-butanol (91.2%).

II. Production of synthesis gas by dry reforming of methane with carbon dioxide

- Preparing some nickel deposited on alumina catalysts, with very small nanoparticle sizes, 2.9 – 3.6 nm and with a very good distribution of the metal on the support. These catalysts have shown very good results when tested in the reforming process of methane with carbon dioxide expressed by methane conversion, carbon dioxide conversion and total yield of transformation of the reactants to carbon monoxide.

- Simulating in Aspen Plus of the process of dry reforming of methane with carbon dioxide for the specific conditions of molar ratios between the reactants that I worked on.

- Developing a gas chromatographic analysis method of gaseous reaction products using a special gas chromatograph for gas analysis – GC-FID+TCD (FID – flame ionization detector and TCD – thermal conductivity detector.

- Conception and realization of a glass T-Y piece for introducing the reactant mixture into the reactor (as well as water and thermocouple).

- Setting up a procedure for the regeneration of spent catalysts, which were used in the dry methane reforming process with carbon dioxide.

- A method for segregating acid sites on the surface of the support, Al_2O_3, in Lewis and Brönsted acid sites. The method uses thermogravimetric desorption of pyridine adsorbed on the acid sites of the support. Then, the infrared spectra with Fourier transform are recorded and interpreted for pyridine also fixed on these acid sites.

- Partial explanation using analyzes such as: (a) X-ray diffraction (XRD), (b) energy dispersive spectroscopy (EDX), (c) nitrogen adsorption-desorption isotherms, (d) Fourier infrared spectra for pyridine fixed on the acid sites of the catalysts (FTIR), (e) transmission electron microscopy (TEM), of process control parameters.

- Carrying out endurance tests for the three catalysts prepared in the process of dry reforming of methane with carbon dioxide with heating supplied conventionally (electrically) for 1200 minutes at a temperature of 850 °C, in which notable results were obtained (minimum value/maximum value): methane conversion values above 95% (min. 95/ max. 100%), carbon dioxide values above 85% (min. 85/ max. 93.2%) and conversion yields of reactants into carbon monoxide over 80% (min. 80/max. 98%).

- Assembling a monomode microwave applicator adapted to the requirements of testing catalysts for dry reforming of methane with carbon dioxide with heating provided by a microwave field and temperature measurement with an infrared sensor.

- Assembling a monomode microwave applicator adapted to the requirements of testing catalysts for dry reforming of methane with carbon dioxide with heating provided by a microwave field and temperature measurement with a thermocouple and an infrared sensor. A LibreVNA vector network analyzer was used to adapt the applicator configuration to avoid the emission of microwave energy by the metal sheath of the thermocouple (which acts as a microwave antenna).

- Carrying out an extended endurance test for the catalyst prepared by coprecipitation in the process of dry methane reforming with carbon dioxide with heating provided by a microwave field for 2000 minutes and then continuing with heating provided conventionally (electrically) also for the duration of 2000 minutes.

- Demonstrating the fact that the catalytic activity of the catalyst prepared by coprecipitation and tested both with conventional heating (constant temperature at 800 °C) and with heating in a microwave field, is higher for heating in the microwave field.

- Demonstrating, through long-term endurance tests (with conventional heating and with heating in a microwave field) that a high-performance catalyst has been obtained for the catalysis of dry methane reforming process with carbon dioxide.

III. Extraction of recoverable active principles from Liquorice technological waste left after conventional extraction

- Using a technological waste of Liquorice root remaining after the conventional extraction in aqueous medium (carried out at an industrial partner) for the recovery of another fraction of active principles and producing lignin and sugars.

- Using Dual Frequency Reactor (DFR) equipment for ultrasonic treatment and Synthwave equipment for microwave treatment of Liquorice technological waste.

- Developing a valorization strategy and method of: (a) glycyrrhizic acid extraction, (b) delignification and (c) enzymatic hydrolysis for a technological waste of Liquorice obtained after conventional extraction in aqueous phase.

- Carrying out a degradation study of glycyrrhizic acid during ultrasound and microwave treatments.

DISSEMINATION OF RESEARCH RESULTS

PUBLISHED ARTICLES

1. **Chisega-Negrilă C-G**, Diacon A, Călinescu I, Vînătoru M (2019), Conversion of n-butanol to n-butyraldehyde – screening of copper catalysts, U.P.B. Sci. Bull., series B 81(2) _ CiteScore 2021 – 0.8

2. Staicu V, Luntraru C, Călinescu I, **Chisega-Negrilă C-G**, Vînătoru M, Neagu M, Gavrilă A, Popa I (2021), Ultrasonic or microwave cascade treatment of medicinal plant waste, Sustainability, 13, 12849 _ IF 3.889

3. **Chisega-Negrilă C-G**, Diacon A, Călinescu I, Vînătoru M, Berger D., Matei C, Vasilievici G (2022), On the ultrasound-assisted preparation of Cu/SiO_2 system as a selective catalyst for the conversion of biobutanol to butanal, Chemical Papers 76 (3) 1443-1455 _ IF 2.097

PARTICIPATION IN CONFERENCES

1. Chisega-Negrilă C-G, Călinescu I, Diacon A, Trifan A (2017), Supported nanocatalysts and their testing in organic synthesis to obtain bioproducts, 20th RICCCE, Poiana Brașov, September 6-9

2. Chisega-Negrilă A-M, Chisega-Negrilă C-G (2018), Building motivation by involving students in lab-related tasks through software and automatizations, 14th ELSE, București, April 19-20

BIBLIOGRAPHY

1. Campanati, M., G. Fornasari, and A. Vaccari, *Fundamentals in the preparation of heterogeneous catalysts.* Catalysis Today, 2003. **77**(4): p. 299-314.
2. Perego, C. and P. Villa, *Catalyst preparation methods.* Catalysis Today, 1997. **34**: p. 281-305.
3. Chaturvedi, S., N.D. Pragnesh, and N.K. Shah, *Applications of nano-catalyst in new era.* Journal of Saudi Chemical Society, 2012. **16**(3): p. 307-325.
4. Munnik, P., P.E. de Jongh, and K.P. de Jong, *Recent developments in the synthesis of supported catalysts.* Chem Rev, 2015. **115**(14): p. 6687-718.
5. Bang, J.H. and K.S. Suslick, *Applications of ultrasound to the synthesis of nanostructured materials.* Adv Mater, 2010. **22**(10): p. 1039-59.
6. Dias, H.V.R., B.I. Kharisov, and O.V. Kharissova, *Study of High-Power Ultrasound-Assisted Processes Using Copper-Containing Precursors in Aqueous Media.* Synthesis and Reactivity in Inorganic, Metal-Organic, and Nano-Metal Chemistry, 2016. **46**(11): p. 1605-1612.
7. Suslick, K.S., et al., *Sonochemical synthesis of nanostructured catalysts.* Materials Science and Engineering 1995. **A204**: p. 186-192.
8. Saez, V. and T.J. Mason, *Sonoelectrochemical synthesis of nanoparticles.* Molecules, 2009. **14**(10): p. 4284-99.
9. Leonelli, C. and T.J. Mason, *Microwave and ultrasonic processing: Now a realistic option for industry.* Chemical Engineering and Processing: Process Intensification, 2010. **49**(9): p. 885-900.
10. Mason, T., *Advances in Sonochemistry, Volume 3*. 1993.
11. Mason, T.J., *Industrial sonochemistry: Potential and practicality.* Ultrasonics, 1992. **30**: p. 192-196.
12. Mason, T.J., *Advances in sonochemistry*. 1996: Elsevier Science.
13. Mason, T.J., *Ultrasound in synthetic organic chemistry.* Chemical Society Reviews, 1997. **26**: p. 443-451.
14. Mason, T.J., *Sonochemistry: current uses and future prospects in the chemical and processing industries.* Philosophical Transactions of the Royal Society A Mathematical, Physical and Engineering Sciences, 1999. **357**(1751): p. 355-369.
15. Cherepanov, P.V., M. Ashokkumar, and D.V. Andreeva, *Ultrasound assisted formation of Al-Ni electrocatalyst for hydrogen evolution.* Ultrasonics Sonochemistry, 2014. **23**: p. 142-147.
16. Saleh, I.A., et al., *A possible general mechanism for ultrasound-assisted extraction (UAE) suggested from the results of UAE of chlorogenic acid from Cynara scolymus L. (artichoke) leaves.* Ultrasonics Sonochemistry, 2016. **31**: p. 330-336.
17. Mitchell, T.M. and F.G. Hammitt, *Asymmetric Cavitation Bubble Collapse.* Journal of Fluids Engineering, 1973. **95(1)**: p. 29-37.
18. Klein, S.J., *Butyraldehyde A2 - Wexler, Philip*, in *Encyclopedia of Toxicology (Third Edition)*. 2014, Academic Press: Oxford. p. 595-596.
19. Luttrell, W.E. and J.W. Tyler, *Butyraldehyde.* Journal of Chemical Health and Safety, 2011. **18**(2): p. 25-26.
20. Liu, K., et al., *Continuous syngas fermentation for the production of ethanol, n-propanol and n-butanol.* Bioresour Technol, 2014. **151**: p. 69-77.
21. Mascal, M., *Chemicals from biobutanol: technologies and markets.* Biofuels, Bioprod. Bioref. , 2012: p. 11.
22. Shutt, J. and J. Brinen, *Converting propylene in an oxygenate-contaminated propylene stream to non-polymerization derivative products*. 2005, Google Patents.
23. Matthias Beller, B.C., Carl D. Frohning, Christian W. Kohlpaintner, *Progress in hydroformylation and carbonylation.* Journal of Molecular Catalysis A:, 1995. **104**: p. 17-85.
24. Ndaba, B., I. Chiyanzu, and S. Marx, *n-Butanol derived from biochemical and chemical routes: A review.* Biotechnol Rep (Amst), 2015. **8**: p. 1-9.
25. Calinescu, I., et al., *Nanoparticles synthesis by electron beam radiolysis.* Central European Journal of Chemistry, 2014. **12(7)**: p. 774-781.
26. Halawy, S.A., *Unpromoted and K_2O-Promoted Cobalt Molybdate as Catalysts for the Decomposition of Acetic Acid.* Chemical Monthly, 2003. **134**: p. 371-380.
27. Mekhemer, G.A., et al., *Qualitative and Quantitative Assessments of Acid and Base Sites Exposed on Polycrystalline MgO Surfaces: Thermogravimetric, Calorimetric, and in-Situ FTIR Spectroscopic Study Combination.* Journal of Physical Chemistry B, 2004. **108(35)**: p. 13379–13386
28. Osman, A.I., et al., *Effect of precursor on the performance of alumina for the dehydration of methanol to dimethyl ether.* Applied Catalysis B: Environmental, 2012. **127**: p. 307-315.
29. Lomate, S., A. Sultana, and T. Fujitani, *Effect of SiO_2 support properties on the performance of Cu-SiO_2 catalysts for the hydrogenation of levulinic acid to gamma valerolactone using formic acid as hydrogen source.* Catalysis Science & Technology, 2017.
30. Zaki, M., et al., *In situ FTIR spectra of pyridine adsorbed on SiO_2–Al_2O_3, TiO_2, ZrO_2 and CeO_2: general considerations for the identification of acid sites on surfaces of finely divided metal oxides.* Colloids and Surfaces A: Physicochemical and Engineering Aspects, 2001. **190**: p. 261-274.

31. Wong, K.N. and S.D. Colson, *The FT-IR Spectra of Pyridine and Pyridine-d_5.* Journal of Molecular Spectroscopy, 1984. **104**(1): p. 129-151.
32. Kuterasiński, Ł., et al., *Reduction and Oxidation of Cu Species in Cu-Faujasites Studied by IR Spectroscopy.* Molecules, 2020. **25**(4765).
33. Herzberg, G., *Molecular Spectra and Molecular Structure II*. 1962, New York, 1962: Van Nostrand.
34. Scherrer, P., *Bestimmung der Größe und der inneren Struktur von Kolloidteilchen mittels Röntgenstrahlen.* Nachrichten von der Gesellschaft der Wissenschaften zu Göttingen, Mathematisch-Physikalische Klasse 1918 1918: p. 98-100.
35. Langford, J.I. and A. Wilson, *Scherrer after sixty years: A survey and some new results in the determination of crystallite size.* J. Appl. Crystallogr., 1978. **11(2)**: p. 102–113.
36. Cherepanov, P.V., I. Melnyk, and D.V. Andreeva, *Effect of high intensity ultrasound on Al_3Ni_2, Al_3Ni crystallite size in binary AlNi (50 wt% of Ni) alloy.* Ultrasonics Sonochemistry, 2015. **23**: p. 26-30.
37. Gabriëls, D., et al., *Review of catalytic systems and thermodynamics for the Guerbet condensation reaction and challenges for biomass valorization*. Catalysis Science & Technology, 2015. **5**: p. 27.
38. Keuler, J.N., L. Lorenzen, and S. Miachon, *The dehydrogenation of 2-butanol over copper-based catalysts: optimising catalyst composition and determining kinetic parameters.* Applied Catalysis A: General, 2001. **218**: p. 171-180.
39. Wongpisutpaisan, N., et al., *Sonochemical Synthesis and Characterization of Copper Oxide Nanoparticles.* Energy Procedia, 2011. **9**: p. 404-409.
40. Gawande, M.B., et al., *Cu and Cu-Based Nanoparticles: Synthesis and Applications in Catalysis.* Chem Rev, 2016. **116**(6): p. 3722-811.
41. Dan, M., M. Mihet, and M.D. Lazar, *Hydrogen and/or syngas production by combined steam and dry reforming of methane on nickel catalysts.* International Journal of Hydrogen Energy, 2019.
42. Jabbour, K., *Tuning combined steam and dry reforming of methane for "metgas" production: A thermodynamic approach and state-of-the-art catalysts.* Journal of Energy Chemistry, 2020. **48**: p. 54-91.
43. Rezaei, E. and S. Dzuryk, *Techno-economic comparison of reverse water gas shift reaction to steam and dry methane reforming reactions for syngas production.* Chemical Engineering Research and Design, 2019. **144**: p. 354–369.
44. Metz, B., et al., *IPCC, 2005: IPCC Special Report on Carbon Dioxide Capture and Storage. Prepared by Working Group III of the Intergovernmental Panel on Climate Change [Metz, B., O. Davidson, H. C. de Coninck, M. Loos, and L. A. Meyer (eds.)]. Cambridge*.
45. Cuéllar-Franca, R.M. and A. Azapagic, *Carbon capture, storage and utilisation technologies: A critical analysis and comparison of their life cycle environmental impacts.* Journal of CO2 Utilization, 2015. **9**: p. 82-102.
46. Tophan, S., et al., *Carbon Dioxide, in Ullmann, F., Gerhartz, W. Yamamoto, Y.S., Campbell, F.T., Ulmann's Encyclopedia of Industrial Chemistry, 2014, Wiley-VCH, .* 2014.
47. Kirk, R.E., et al., *Carbon Dioxide in Kirk- Othmer Concise Encyclopedia of Chemical Technology, Wiley & Sons, New York.* 1985.
48. Olah, G.A., *Beyond oil and gas: the methanol economy.* Angew Chem Int Ed Engl, 2005. **44**(18): p. 2636-9.
49. Creutz, C. and E. Fujita, *Carbon Dioxide as Feedstock in National Research Council 2001. Carbon Management: Implications for R & D in the Chemical Sciences and Technology (A Workshop Report to the Chemical Sciences Roundtable). Washington, DC: The National Academies Press.* 2001.
50. Fan, M.-S., A.Z. Abdullah, and S. Bhatia, *Utilization of greenhouse gases through carbon dioxide reforming of methane over Ni–Co/MgO–ZrO2: Preparation, characterization and activity studies.* Applied Catalysis B: Environmental, 2010. **100**(1-2): p. 365-377.
51. Yentekakis, I.V. and G. Goula, *Biogas Management: Advanced utilization for production of renwable energy and added-value chemicals.* Frontiers in Environmental Science, 2017. **5:7**.
52. Papadopoulou, C., H. Matralis, and X. Verykios, *Utilization of Biogas as a Renewable Carbon Source: Dry Reforming of Methane. In: Guczi L., Erdôhelyi A. (eds) Catalysis for Alternative Energy Generation. Springer, New York, NY.* 2012.
53. Dominguez, A., et al., *Biogas to Syngas by Microwave-Assisted Dry Reforming in the presence of char.* Energy & Fuels 2007 2007. **21**: p. 2066-2071.
54. Hassan Amin, M., *A Mini-Review on CO2 Reforming of Methane.* Progress in Petrochemical Science, 2018. **2**(2).
55. Huang, J., et al., *Characterization and Catalytic Activity of CeO2-Ni/Mo/SBA-15 Catalysts for Carbon Dioxide Reforming of Methane.* Chinese Journal of Catalysis, 2012. **33**(4-6): p. 637-644.
56. Huang, J., et al., *Carbon dioxide reforming of methane over Ni/Mo/SBA-15-La2O3 catalyst: Its characterization and catalytic performance.* Journal of Natural Gas Chemistry, 2011. **20**(5): p. 465-470.
57. Huang, T., et al., *Methane reforming reaction with carbon dioxide over SBA-15 supported Ni–Mo bimetallic catalysts.* Fuel Processing Technology, 2011. **92**(10): p. 1868-1875.
58. Jang, W.-J., et al., *H2 and CO production over a stable Ni–MgO–Ce0.8Zr0.2O2 catalyst from CO2 reforming of CH4.* International Journal of Hydrogen Energy, 2013. **38**(11): p. 4508-4512.
59. Jang, W.-J., et al., *A review on dry reforming of methane in aspect of catalytic properties.* Catalysis Today, 2019. **324**: p. 15-26.
60. Jeong, H., et al., *Effect of promoters in the methane reforming with carbon dioxide to synthesis gas over Ni/HY catalysts.* Journal of Molecular Catalysis A: Chemical, 2006. **246**(1-2): p. 43-48.

61. Jin, L., et al., *CO2 reforming of methane on Ni/γ-Al2O3 catalyst prepared by dielectric barrier discharge hydrogen plasma.* International Journal of Hydrogen Energy, 2014. **39**(11): p. 5756-5763.
62. Lavoie, J.M., *Review on dry reforming of methane, a potentially more environmentally-friendly approach to the increasing natural gas exploitation.* Front Chem, 2014. **2**: p. 81.
63. Liu, D., et al., *Carbon dioxide reforming of methane to synthesis gas over Ni-MCM-41 catalysts.* Applied Catalysis A: General, 2009. **358**(2): p. 110-118.
64. Mondal, K., et al., *Dry reforming of methane to syngas: a potential alternative process for value added chemicals-a techno-economic perspective.* Environ Sci Pollut Res Int, 2016. **23**(22): p. 22267-22273.
65. Niu, J., et al., *Methane dry (CO2) reforming to syngas (H2/CO) in catalytic process: From experimental study and DFT calculations.* International Journal of Hydrogen Energy, 2020.
66. Ranjekar, A.M. and G.D. Yadav, *Dry reforming of methane for syngas production: A review and assessment of catalyst development and efficacy.* Journal of the Indian Chemical Society, 2021. **98**(1).
67. Shah, Y.T. and T.H. Gardner, *Dry Reforming of Hydrocarbon Feedstocks.* Catalysis Reviews, 2014. **56**(4): p. 476-536.
68. Singh, R., S.K. Mohapatra, and S.K. Mahla, *Dry reforming of methane using various catalysts in the process: review.* Biomass Conversion and Biorefinery, 2020. **10**: p. 567–587.
69. Usman, M., W.M.A. Wan Daud, and H.F. Abbas, *Dry reforming of methane: Influence of process parameters—A review.* Renewable and Sustainable Energy Reviews, 2015. **45**: p. 710-744.
70. Zhu, J., et al., *Synthesis gas production from CO2 reforming of methane over Ni–Ce/SiO2 catalyst: The effect of calcination ambience.* International Journal of Hydrogen Energy, 2013. **38**(1): p. 117-126.
71. Al-Nakoua, M.A. and M.H. El-Naas, *Combined steam and dry reforming of methane in narrow channel reactors.* International Journal of Hydrogen Energy, 2012. **37**(9): p. 7538-7544.
72. Gao, N., et al., *Syngas production via combined dry and steam reforming of methane over Ni-Ce/ZSM-5 catalyst.* Fuel, 2020. **273**(117702).
73. Huang, B., et al., *Effect of MgO promoter on Ni-based SBA-15 catalysts for combined steam and CO2 reforming of CH4.* Journal of Natural Gas Chemistry 2008. **17**: p. 225-231.
74. Wysocka, I., et al., *Effect of small quantities of potassium promoter and steam on the catalytic properties of nickel catalysts in dry/combined methane reforming.* International Journal of Hydrogen Energy, 2021. **46**(5): p. 3847-3864.
75. Froment, G.F., *Production of synthesis gas by steam- and CO2 reforming of natural gas.* Journal of Molecular Catalysis A: Chemical 2000. **163 (2000)** p. 10.
76. Gangadharan, P., K.C. Kanchi, and H.H. Lou, *Evaluation of the economic and environmental impact of combining dry reforming with steam reforming of methane.* Chemical Engineering Research and Design, 2012. **90**: p. 1956-1968.
77. Luyben, W.L., *Control of parallel dry methane and steam methane reforming processes for Fischer–Tropsch syngas.* Journal of Process Control, 2016. **39**: p. 77-87.
78. Seo, J.G., M.H. Youn, and I.K. Song, *Effect of preparation method of mesoporous Ni–Al2O3 catalysts on their catalytic activity for hydrogen production by steam reforming of liquefied natural gas (LNG).* International Journal of Hydrogen Energy, 2009. **34**(13): p. 5409-5416.
79. Cormos, C.-C., *Evaluation of energy integration aspects for IGCC-based hydrogen and electricity co-production with carbon capture and storage.* International Journal of Hydrogen Energy, 2010. **35**(14): p. 7485-7497.
80. Arbag, H., et al., *Activity and stability enhancement of Ni-MCM-41 catalysts by Rh incorporation for hydrogen from dry reforming of methane.* International Journal of Hydrogen Energy, 2010. **35**(6): p. 2296-2304.
81. Steynberg, A.P. and H.G. Nel, *Clean coal conversion options using Fischer–Tropsch technology.* Fuel, 2004. **83**(6): p. 765-770.
82. Bankar, S.B., et al., *Biobutanol: the outlook of an academic and industrialist.* RSC Advances, 2013. **3**(47): p. 24734.
83. Durre, P., *Fermentative production of butanol-the academic perspective.* Curr Opin Biotechnol, 2011. **22**(3): p. 331-6.
84. Green, E.M., *Fermentative production of butanol--the industrial perspective.* Curr Opin Biotechnol, 2011. **22**(3): p. 337-43.
85. Kumar, M. and K. Gayen, *Developments in biobutanol production: New insights.* Applied Energy, 2011. **88**(6): p. 1999-2012.
86. Nanda, S., et al., *Fermentative production of butanol: Perspectives on synthetic biology.* N Biotechnol, 2017. **37**(Pt B): p. 210-221.
87. Albonetti, S., et al., *Chemicals and fuels from bio-based building blocks.* Wiley-VCH Verlag GmbH & Co (2016), 2016. **I**.
88. Dürre, P., *Biobutanol: An attractive biofuel.* Biotechnol. J., 2007. **2**: p. 10.
89. Trindade, W.R.d.S. and R.G.d. Santos, *Review on the characteristics of butanol, its production and use as fuel in internal combustion engines.* Renewable and Sustainable Energy Reviews, 2017. **69**: p. 642-651.
90. E4tech, RE-CORD, and WUR, *"From the Sugar Platform to biofuels and biochemicals". Final report for the European Commission - contract No. ENER/C2/423-2012/SI2.673791*. 2015.
91. Teuner, S.C., P. Neumann, and F. von Linde, *The Calcor Standard and Calcor Economy Processes.* Oil Gas European Magazine, 2001. **3**.
92. van Diepen, A.E., et al., *Contribution of catalysis towards the reduction of atmosferic air pollution-CO2-CFCs-N2O-O3, chapter 11 in book - Janssen, F.J.J.G., van Santen, R.A., Catalytic Science Series, Environmental Catalysis, volume 1, OZONE, page: 219-256, Imperial College Press, ISBN: 978-1-86094-125-2, 978-1-84816-061-3.* 1999. **10.1142/p106**.

93. Thommes, M., et al., *Physisorption of gases, with special reference to the evaluation of surface area and pore size distribution (IUPAC Technical Report).* Pure and Applied Chemistry, 2015. **87**(9-10).
94. McNaught, A.D. and A. Wilkinson, *Compendium of Chemical Terminology - IUPAC Recommendations, Gold Book*. Second Edition ed. 2021.
95. Rahmanpour, O., A. Shariati, and M.R. Khosravi-Nikou, *New Method for Synthesis Nano Size γ-Al_2O_3 Catalyst for Dehydration of Methanol to Dimethyl Ether.* International Journal of Chemical Engineering and Applications, 2012. **3**(2).
96. Song, K.H., et al., *Effect of the Ni/Al Ratio on the Performance of $NiAl_2O_4$ Spinel-Based Catalysts for Supercritical Methylcyclohexane Catalytic Cracking.* Catalysts, 2021. **11(3)**(323).
97. Chelliah, M., J.B.B. Rayappan, and U.M. Krishnan, *Synthesis and Characterization of Cerium Oxide Nanoparticles by Hydroxide Mediated Approach.* Journal of Applied Sciences, 2012. **12**(16): p. 1734-1737.
98. Al-Mubaddel, F.S., et al., *Optimizing acido-basic profile of support in Ni supported La_2O_3+Al_2O_3 catalyst for dry reforming of methane.* International Journal of Hydrogen Energy, 2021. **46**(27): p. 14225-14235.
99. Junke, X.U., et al., *Characterization and analysis of carbon deposited during the dry reforming of methane over Ni/La_2O_3/Al_2O_3 catalysts.* Chisese Journal of Catalysis, 2009. **11**: p. 1076-1084.
100. Chein, R.Y. and W.Y. Fung, *Syngas production via dry reforming of methane over CeO_2 modified Ni/Al_2O_3 catalysts.* International Journal of Hydrogen Energy, 2019. **44**: p. 14303-14315.
101. Wong, K.N. and S.D. Coloson, *The FT-IR Spectra of Pyridine and Pyridine-d5.* Journal of Molecular Spectroscopy, 1984. **104**(1): p. 129-151.
102. Fitzgerald, M.E., V. Griffing, and J. Sullivan, *Chemical Effects of Ultrasonics—``Hot Spot'' Chemistry.* The Journal of Chemical Physics, 1956. **25**(5): p. 926.
103. Mathews, S.L., J. Pawlak, and A.M. Grunden, *Bacterial biodegradation and bioconversion of industrial lignocellulosic streams.* Applied Microbiology and Biotechnology, 2015. **99**(7): p. 2939-54.
104. Klass, D., *Biomass for Renewable Energy, Fuels and Chemicals*. 1998: Academic Press (Elsevier).
105. European Commission, a., *Biomass - Green energy for Europe*. 2005: Luxembourg.
106. Fardad, K., et al., *Biodegradation of Medicinal Plants Waste in an Anaerobic Digestion Reactor for Biogas Production.* Computers, Materials & Continua, 2018. **55**(3): p. 381-392.
107. Fernandez, A., et al., *Kinetic analysis and thermodynamics properties of air/steam gasification of agricultural waste.* Journal of Environmental Chemical Engineering, 2020. **8**(4): p. 103829.
108. *Sustainable and optimal use of biomass for energy in the EU beyond 2020*. 2017, European Commision: Wien.
109. Avelino Corma, S.I., and Alexandra Velty, *Chemical Routes for the Transformation of Biomass into Chemicals.* Chem. Rev., 2007. **107**: p. 2411-2502.
110. Biddy, M., C. Scarlata, and C. Kinchin, *Technical Report NREL/TP-5100-65509 - Chemicals from Biomass: A Market Assessment of Bioproducts with Near-Term Potential* 2016, NREL.
111. Climent, M.J., A. Corma, and S. Iborra, *Conversion of biomass platform molecules into fuel additives and liquid hydrocarbon fuels.* Green Chemistry, 2014. **16**(2): p. 516.
112. Fiorentino, G., M. Ripa, and S. Ulgiati, *Chemicals from biomass: technologicalversusenvironmental feasibility. A review.* Biofuels, Bioproducts and Biorefining, 2017. **11**(1): p. 195-214.
113. Hamelinck, C., et al., *Production of FT transportation fuels from biomass; technical options, process analysis and optimisation, and development potential.* Energy, 2004. **29**(11): p. 1743-1771.
114. Kim, S.M., et al., *Conversion of biomass-derived butanal into gasoline-range branched hydrocarbon over Pd-supported catalysts.* Catalysis Communications, 2011. **16**(1): p. 108-113.
115. SAVAGE, N., *The ideal biofuel: A biomass-based fuel needs to be cheap and energy dense. Gasoline sets a high standard.* Nature, 2011. **Vol. 474**: p. S9-S11.
116. Shanks, B.H. and P.L. Keeling, *Bioprivileged molecules: creating value from biomass.* Green Chem., 2017. **19**(14): p. 3177-3185.
117. Werpy, T. and G. Petersen, *Top Value Added Chemicals from Biomass Volume I—Results of Screening for Potential Candidates from Sugars and Synthesis Gas.* U.S. Department of Energy -Biomass, 2004: p. 1-76.
118. Zhang, Q.W., L.G. Lin, and W.C. Ye, *Techniques for extraction and isolation of natural products: a comprehensive review.* Chinese Medicine, 2018. **13**: p. 1-26.
119. do C. de Sousa, C.B., et al., *Greener ultrasound-assisted extraction of bioactive phenolic compounds in Croton heliotropiifolius Kunth leaves.* Microchemical Journal, 2020. **159**: p. 105525.
120. Gasmalla, M.A., R. Yang, and X. Hua, *Extraction of rebaudioside-A by sonication from Stevia rebaudiana Bertoni leaf and decolorization of the extract by polymers.* J Food Sci Technol, 2015. **52**(9): p. 5946-53.
121. Jaitak, V., B. Bikram Singh, and V.K. Kaul, *An efficient microwave-assisted extraction process of stevioside and rebaudioside-A from Stevia rebaudiana (Bertoni).* Phytochem Anal, 2009. **20**(3): p. 240-5.
122. Mason, T. and M. Vinatoru, *The Extraction of Natural Products using Ultrasound or Microwaves*. Vol. 15. 2011. 237-247.
123. Pinela, J., et al., *Optimization of microwave-assisted extraction of hydrophilic and lipophilic antioxidants from a surplus tomato crop by response surface methodology.* Food and Bioproducts Processing, 2016. **98**: p. 283-298.
124. Priecel, P. and J.A. Lopez-Sanchez, *Advantages and Limitations of Microwave Reactors: From Chemical Synthesis to the Catalytic Valorization of Biobased Chemicals.* ACS Sustainable Chemistry & Engineering, 2018. **7**(1): p. 3-21.

125. Sombatpraiwan, S., et al., *Optimization of microwave-assisted alkali pretreatment of cassava rhizome for enhanced enzymatic hydrolysis glucose yield.* Food and Energy Security, 2019. **8**(4): p. 1-15.
126. Staicu, V., Luntraru, C. , Calinescu, I., Chisega-Negrila, C.-G., Vinatoru, M., Neagu, M., Gavrila, A.I., Popa, I., *Ultrasonic or Microwave Cascade Treatment of Medicinal Plant Waste.* Sustainability, 2021. **13**(12849).
127. Schoepke, T., *Glycyrrhiza*, in *Hagers Handbuch der Pharmazeutischen Praxis*, Hagers, Editor., Springer: Berlin, Heidelberg.
128. Meier, B., Meier-Liebi, M., *Salix*, in *Hagers Handbuch der Pharmazeutischen Praxis*, Hagers, Editor., Springer: Berlin, Heidelberg.
129. Cygan, F.-C., Frohne, D., Hötzel, C., Nagell, A., Pfänder, H.J., Willuhn, G., Buff, W., , *Liquiritiae radix - Liquorice*, in *Teedrogeen. Ein Handbuch für die Praxis auf wissenshaftlicher Grundlage*, M. von Wichtl, Editor. 1984: Wissenschaftiche Verlagsgesellschaft mbH, Birkenwaldstrasse 44, D-70191 Stuttgard, Germany. p. 301-304.
130. Cygan, F.-C., Frohne, D., Hötzel, C., Nagell, A., Pfänder, H.J., Willuhn, G., Buff, W., , *Salicis cortex - Willow bark*, in *Teedrogeen. Ein Handbuch für die Praxis auf wissenshaftlicher Grundlage*, M. von Wichtl, Editor., Wissenschaftiche Verlagsgesellschaft mbH, Birkenwaldstrasse 44,: D-70191 Stuttgard, Germany. p. 437-439.